Archives of Mining Sciences **47**, 2 (2002) 205–253

STANISLAW NAGY*

CAPILLARY ADSORPTION EFFECTS IN GAS CONDENSATE SYSTEMS IN TIGHT ROCKS

ZJAWISKA ADSORPCYJNE I KAPILARNE W UKŁADACH GAZOWO-KONDENSATOWYCH W ZBITYCH SKAŁACH POROWATYCH

This paper summarizes some experimental work performed with a porous media core in the PVT cell and discusses impact adsorption/capillarity and gravity phenomena on the Vapour-Liquid Equilibria (VLE) properties of gas condensate and near-critical oil systems. The influence of adsorption/capillary effects is investigated theoretically using the cubic equation of state (CEOS) and a modified Kelvin equation. Computation of saturation-curve movement under the curvature of porous media and other volumetric end phase equilibrium parameters are discussed.

Key words: adsorption, Kelvin, cubic equation of state, porous media, condensate gas, vapour-liquid equilibria

W klasycznym ujęciu termodynamicznym w zakresie własności PVT i równowagi fazowej ciecz–para (VLE) pomijany jest efekt segregacji grawitacyjnej, oddziaływań zjawisk kapilarnych czy wpływ zmienności temperatury złożowej na ciśnienie nasycenia (ciśnienie rosy — kondensacji, i ciśnienie pęcherzyków — wrzenia), temperaturę krikondenternu czy ciśnienie krikondenbaru. Przypomnieć należy sprzeczne wnioski dotyczące zakresu oddziaływania struktury porowej na zjawisko zmienności składu spowodowane np. kondensacją kapilarną. Badania rosyjskie i amerykańskie (Trebin, Zadara 1968; Sadyk-Zada 1963, 1968; Tindy, Reynal 1966) wykazywały istotny wpływ zjawisk kapilarnych na krzywą nasycenia. Trebin i Zadara (1968) pokazali, że ciśnienia nasycenia układu gazowo-kondensatowego w obecności ośrodka porowatego są o 10–15% wyższe od obserwowanych w zwykłej komorze PVT. Tindy i Reynol (1966) wskazali, że ciśnienia nasycenia ropy naftowej w obecności ośrodka porowatego są o kilka procent wyższe od ciśnień pomiarowych bez obecności skały porowej. Inne badania amerykańskie i kanadyjskie (Smith, Yarborough 1968; Weinang, Cordell 1949; Oxford i Huntington 1953; Singmund et al. 1973) wskazują na brak istotnego wpływu wielkości średniego promienia porowego na wielkość ciśnienia nasycenia.

Sigmund et al. (1974) pokazali, że przyczyną powodującą rzekomy wpływ struktury na ciśnienie nasycenia jest fakt, iż płyn nie był przemieszczany w ośrodku porowatym i dlatego wykonali oni

* WYDZIAŁ WIERTNICTWA, NAFTY I GAZU, AKADEMIA GÓRNICZO-HUTNICZA, 30-059 KRAKÓW, AL. MICKIEWICZA 30; e-mail: nagy@agh.edu.pl

analogiczne badania z recyrkulacją płynu węglowodorowego przez ośrodek porowaty. Efekt kapilarny jest istotny w przypadku bardzo dużych krzywizn (tzn. promienie porowe rzędu 10^{-5}–10^{-7} cm). Dodatkowo Sigmund i inni twierdzą, że takie krzywizny mogą być niedostępne dla układów o zwilżalności hydrofilnej, w których istnieją duże wartości nasycenia wodą resztkową S_{wi}.

Z kolei badania chińskie Yan (1988) wskazują na przesunięcie w górę krzywych nasycenia. Badania te wskazują, że proces kondensacji wstecznej jest przyspieszany, a punkt rosy ma ciśnienie wyższe w odniesieniu do układu bez ośrodka porowatego.

Z kolei inni Chińczycy Zu i Huang (1988) wyciągnęli konkluzję, że ciśnienie rosy w układzie ośrodka porowatego było nieco niższe niż w układzie bez ośrodka porowatego, a w pobliżu punktu krytycznego stopień wpływu był mały. W ocenie autora część badań eksperymentalnych prowadzona była przy wykorzystaniu ośrodka porowatego o cechach nie występujących często w warunkach złożowych. Zastrzeżenia można mieć szczególnie do wyboru piasku czy słabo zwięzłych piaskowców o przepuszczalności powyżej 250 mD. Kwestią dyskusyjną jest przyjęcie warunków dynamicznej wymiany płynów (cyrkulacji) w komorze PVT w trakcie wykonywania pomiarów ciśnienia nasycenia (Sigmund et al. 1974). Otwartą kwestią jest również, zdaniem autora, występowanie układów o małym promieniu hydraulicznym (poniżej 10 μm) w przyrodzie w skałach poniżej 3000 m o zwilżalności hydrofobowej, co kwestionuje Sigmund (1974). Rozważania dotyczące występowania zwilżalności hydrofilnej w skałach o biogenicznym pochodzeniu gazu powstałego na skutek degeneracji materii organicznej przez organizmy anaerobowe i w skałach o termogenicznym pochodzeniu gazu powstałego przez biodegradację związanych ciekłych węglowodorów oraz identyfikacji *in situ* typu zwilżalności w takich układach znaleźć można w pracy Debrandesa i Bassiouniego (1990), Sassena (1988). W złożach głębokich poniżej 3000 m z uwagi na panujące warunki ciśnienia i temperatury resztki bitumiczne i siarka mogą pokrywać pory filmami hydrofobowymi. Woda w tym przypadku nie jest wodą związaną. Również opinie Lee (1989) i Guo (1986) potwierdzają konieczność uwzględnienia oddziaływań kapilarnych dla skał głęboko położonych o niskiej przepuszczalności.

Zjawiska adsorpcji mają znaczny wpływ na rozkład zasobów złóż gazu i ropy, gazu ziemnego z pokładów węgla czy też złóż geotermalnych. Proces adsorpcji (desorpcji) wewnątrz ośrodka porowatego różni się w znacznym stopniu od adsorpcji na powierzchni z dwóch zasadniczych powodów (rys. 1):

- występowania naturalnej krzywizny porów, w których może występować zjawisko kondensacji kapilarnej,
- możliwości dostępu do określonych porów są ograniczone wpływem topologii sieci połączeń, co powoduje zjawisko blokowania niektórych porów.

Zjawiska adsorpcji zachodzące w ośrodkach porowatych były przedmiotem wielu monografii (m.in. Defay, Prigogine 1966; Adamson 1990; Dullien 1992). Stan prac w zakresie adsorpcji ocenić można w artykułach Shapiro, Stenby (1996, 2000, 2001), Guo et al. (1966) oraz Satik, Horne, Yortsos (1995), Yortsos, Stubos (2001). Zjawisko adsorpcji i wpływ sił kapilarnych uzupełniają się wzajemnie, w obszarach gdzie napięcie powierzchniowe zanika pojawia się większy wpływ sił adsorpcyjnych (np. w pobliżu punktu krytycznego). Wyróżnić należy dwa rodzaje modeli adsorpcyjnych: modele opisujące adsorpcję w pojedynczej kapilarze i modele uwzględniające krzywiznę ośrodka porowatego składającego się z wielu porów. Na rysunku 2 pokazano najważniejsze charakterystyczne zjawiska dotyczące adsorpcji i kondensacji w ośrodku porowatym w pobliżu krzywej nasycenia. Wydaje się, że najlepiej opisuje te zjawiska model FHH (Frankela-Halsey'a-Hilla) (Adamson 1990), przynajmniej w wysokich i średnich zakresach ciśnień. Jako alternatywę modelu FHH można przyjąć model de Boera et al. (1956). Kondensację kapilarną opisuje się zwykle zmodyfikowanym równaniem Kelvina (Adamson 1990) (równania 3–6). Odpowiednie badania eksperymentalne grubości filmu adsorpcyjnego w ośrodku porowatym w wysokich ciśnieniach zamieszczono na podstawie pracy Gregga i Singa (1982) (tabl. 2 i rys. 3). Model równowagi termodynamicznej ciecz–para w ośrodku porowatym przedstawiono w równaniach 8–18. Jego modyfikacja w postaci zmiany sposobu liczenia stałej równowagi fazowej K jest przedstawiona w wyprowadzeniu w równaniach 19–24. Równanie 24 pokazuje zmianę fugatywności składnika układu w fazie ciekłej związanego z krzywizną układu. W równaniach 25–27 pokazano nowe kryteria dla obliczania równowagi ciecz–para z uwzględnieniem kondensacji kapilarnej, zaś równania 28 i 29 definiują nową postać stałej równowagi ciecz–para w funkcji zarówno składu układu, ciśnienia i temperatury, jak również średniego promienia kapilarnego (zdefiniowanego

poprzez równanie Laplace'a). Przedstawiony został nowy algorytm obliczenia krzywej rosy kondensacji kapilarnej w zbitych skałach porowatych. Przedstawiono nową postać znanego równania bilansowego Rachforda-Rice'a dla obszaru kondensacji kapilarnej (rów. 30). Wyprowadzono nową postać kryterium płaszczyzny stycznej Gibbsa dla kondensacji kapilarnej na podstawie modeli Michelsena (1982a). Teoretyczne wyprowadzenia zastosowano praktycznie do obliczeń równowagowych dla trzech układów gazowo-kondensatowych i ropy naftowej (mixture 1–3). Obliczenia wykonano przy użyciu dwóch podobnych równań stanu typu Penga-Robinsona (1976). Zastosowano równania VTPT (Tai-Chen 1998) oraz Magoulasa, Stamatakiego (1990). Do obliczeń wykorzystano również model Whitsona (1990) rozdzielający nieznany skład frakcji C_{7+} na szereg pseudoskładników (do C_{20+}), co umożliwiło znaczne zwiększenie dokładności obliczeń. Krytyczne parametry otrzymanych pseudoskładników określano w oparciu o korelacje Sima, Daubera (1980), Razi, Daubera (1980) i Wina (1957). Obliczenia napięcia powierzchniowego przeprowadzono w oparciu prace Fanchiego (1990), Danesha et al. (1991), testując model na danych Firozabadiego et al. (1988) (tabl. 12). Na rysunkach 6–32 przedstawiono wpływ zakrzywienia powierzchni porowych i adsorpcji na własności układu ciecz–para dla trzech wymienionych składów w różnych ciśnieniach i temperaturach. Wpływ zakrzywienia powierzchni jest zauważalny dla promienia porowego mniejszego niż 10^{-5} cm i jest znaczny w przypadku promienia większego niż 10^{-7} cm. Obserwuje się widoczne przesunięcie punktu krikondentermu w odniesieniu do układów gazowo-kondensatowych (rys. 27), a krzywa nasycenia jest bardziej wypukła. Przesunięcie obserwowane w odniesieniu do składu nr 3 wynosiło 13°C. W odniesieniu do układów lekkiej ropy naftowej obserwuje się obniżenie krzywej nasycenia (krzywej pęcherzyków) (rys. 15, 16) nawet o 23 bary (w odniesieniu do składu 2). Jeśli chodzi o zmianę składu gazu, największe zmiany obserwuje się w odniesieniu do metanu i węglowodorów ciężkich (do 13% w fazie gazowej). W fazie ciekłej obserwuje się przyrost zawartości metanu i spadek zawartości węglowodorów ciężkich (nawet o 17%). Zmiany w składzie węglowodorów C_2–C_6 są nieznaczne. Obserwowany wypływ zjawisk kapilarnych i adsorpcyjnych na gęstość fazy ciekłej jest znaczący. Obserwowano redukcję gęstości od 0,57 do 0,49 g/cm^3. Wynik ten jest związany ze wzrostem zawartości metanu w fazie ciekłej o 14%.

Jak pokazano w artykule, obserwowane efekty kapilarne i adsorpcyjne mają bardzo duży wpływ na zachowanie się układów dwufazowych w przypadku skał zwięzłych o średnim promieniu porowych mniejszym niż $150 \cdot 10^{-8}$ m, co odpowiada efektywnej przepuszczalności skał poniżej $0{,}5 \cdot 10^{-3}$ μm^2 (0,5 mD). Część zasobów gazu kondensowanego w tych złożach zostanie na stałe zaadsorbowana i desorpcja części zasobów może nastąpić dopiero w ostatnim etapie eksploatacji złoża

Słowa kluczowe: adsorpcja, ciśnienie kapilarne, równanie Kelvina, równanie stanu, środek porowaty, gaz kondensatowy, równowaga ciecz–para

Nomenclature

A, B, C — coefficients in Peng-Robinson EOS,
a, b, t — coefficients in Peng-Robinson EOS,
ϕ — fugacity,
k — binary interaction constant (BIC),
nc — number of components,
p — pressure,
R — universal gas constant,
x — mole fraction of component in liquid phase,
y — mole fraction of component in vapour phase,
v — molar volume,
ω — Pitzer's acentric factor,

z — mole fraction of component in system,
$\acute{R}$ — fugacity coefficient,
β — phase mole fraction,
t_e — critical film thickness,
p_v^{∞} — vapour saturation pressure at flat surface,
p_v — actual vapour pressure,
r — capillary radius,
σ — interfacial surface tension,
V_L — liquid volume,
R — gas constant,
T — temperature,
ΔH_{vl}^{E} — enthalpy of vaporisation,
C^{E} — integration constant,
r_h — generalised hydraulic pore radius,
h_g — shape pore generalisation factor,
μ_i — chemical potential of i-component,
μ_i^{L}, μ_i^{V} — chemical potential of i-component adequately: free liquid, vapour,
μ_i^{Lad}, μ_i^{Vad} — chemical potential of i-component adequately: adsorption liquid, adsorption vapor,
Z^{v}, Z^{L} — vapour and liquid phase compressibility factor,
E — empirical dimensionless constant,
π_i — parachor of i-component,
Nv — vapour-phase mole fraction,
$\overline{V}_i^{L}$ — partial molar liquid component volume,
$\varepsilon_i = \dfrac{\overline{V}_i^{L}}{RT}$ — component Poynting factor.

Indexes

c — critical parameter,
i — i-component,
j — j-component,
l — liquid phase,
n — standard condition,
v — vapour phase.

1. Introduction

Natural-state modelling of a hydrocarbon and geothermal reservoir may be useful in explaining geological heterogeneity and anomalies. Such modelling need be not complicated and laborious. The traditional attitude to flat vapour-liquid thermodynamics may be extended to curved surfaces with gravity and adsorption/capillary condensation effects. It is said that surface interactions in porous media are important in the very narrow capillary radius within the micropores. The principal work of Defay,

Prigogine (1966) shows the necessary to include the lowering vapor pressure of pure components in porous media with an average radius lower than 10^{-5} cm.

The fully thermodynamic analysis of a reservoir hydrocarbon system is impossible because of the large influence of environmental factors. Such factors may be divided into the following classes, according to their features:

Spatial variety of initial (original) reservoir fluid properties induced by (Tissot, Welte 1978; Lee 1989):

I. Thermodynamic factors:
   a) local temperature,
   b) local pressure,
   c) local composition,
   d) slope of reservoir bottom and top layers (gravity forces),
   e) curvature of porous media (capillary forces).

II. Factors associated with the thermodynamic phenomena:
   a) thermal gradients (induced thermal convection — natural or forced),
   b) molecular diffusion.

III. Factors related directly to the porous media:
   a) heterogeneity,
   b) faults (slowing down of equilibrium process),
   c) wettability.

IV. Factors connected with the hydrocarbon accumulation and generation processes:
   a) genesis,
   b) migration,
   c) reservoir traps.

To include all of the above factors is not possible in the reservoir simulation model. The factors of groups III and IV are not particularly useful because of specific features of individual hydrocarbon accumulation. The building of a thermodynamic reservoir model with features of groups I and II and with some selected features from group III may be possible for the "virgin" (i.e. before exploitation) states. This paper describes some of reservoir fluid/porous rock systems including some of features of the first group for the gas-condensate in tight rocks.

2. Solid-hydrocarbon capillary interaction in the porous media

The interface between phases (i.e. gas, condensate, brine) in a porous media is not flat (Fig. 1). The capillarity and gravity segregation effects on the pressure–volume–temperature (PVT) and vapour liquid equilibria (VLE) properties of the reservoir fluid are omitted in the classical thermodynamic analysis. The variation of reservoir temperature in the system is passed over, although the last analysis confirms the necessity to include these effects in some cases (Holt et al. 1983; Wheaton 1988; Creek and Sakrader 1985; Montel and Gouel 1985; Riemans et. al. 1988; Neveux et al. 1988; Hoeier and

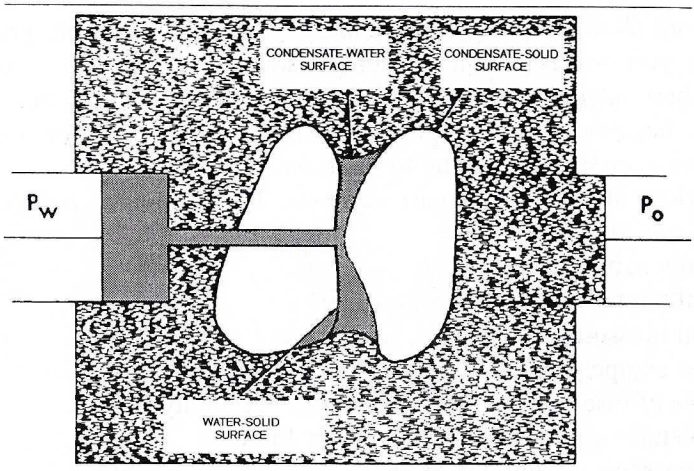

Fig. 1. Idealized model of fluid displacement in a porous media

Rys. 1. Wyidealizowany model wypierania płynu w ośrodku porowatym

Whitson 2000). Such classical analyses may be found in many works: Leverett (1941), Edmister (1961, 1974), McCain (1990), Ahmed (1989), Greenkorn (1983).

In some cases characteristics of porous-media equilibrium conditions the influence of interface curvature should be taken into account (Fig. 1). In the range of laboratory PVT-VLE research the additional effect of capillarity is omitted in the case of the saturation phase envelope.

Below are summarised limited experiences regarding the interaction of porous structure for changeability of composition in the presence of a sandstone reservoir core. The Russian authors Trebin and Zadora (1968) reported a strong influence of the porous media on the dew-point pressure and vapour-liquid equilibria (VLE) of the condensate system. The porous media used in this experiment was a silica-sand mixture (0.215/0.3 mm diameter) ground by a cutter-pulverizer. They used three samples with surface area respectively 563, 1307 and 3415 cm^2 , permabilities 5.6 μm^2 , $612 \cdot 10^{-3}$ μm^2 , $111 \cdot 10^{-3}$ μm^2 and porosities 34, 31.4 and 29.8%. According to the conclusions from this paper the dew–point pressure increases when the surface area of the porous media increases. The observed effect was a 10–15% increase of the dew--point pressure in this system. The observed effect was lessened when the temperature increased. A similar observation was recorded by Sadyk and Zade (1963, 1968).

The research by the French scientists Tint and Raynal (1966) confirm that the bubble pressure of two reservoir crude oils, both in an open space (PVT cell) with grain size in the 16-200 m range were higher by 7 and 4 bar (121 bar vs 128 bar) compared to a PVT cell without porous media.

Other American and Canadian researches (Smith, Yarborough (1968), Weinaug, Cordell (1949), Oxford, Huntington (1953), Sigmund et al. (1973)) indicate that there is no evidence of influence of average capillary porous media on the saturation

pressure. Weinaug and Cordell's (1949) work shows that for the methane-n butane and ethane-n pentane system there is no difference due to the presence of sand in the PVT cell. Oxford and Huntington (1953) showed that during the evaporation of n-hexane during nitrogen injection there was no significant effect on the porous media.

Smith and Yarborough (1968) indicate in their paper about wettability that the porous structure has little impact on the vaporisation process of the liquid phase in the rock.

Sigmund et al. (1974) analysed the laboratory work done by Trebin and Zadora and they concluded that the main reason for the hypothetical impact of the porous structure on the saturation pressure was the lack of fluid circulation in the cell. They performed an analogy experiment with fluid flow through core in the PVT cell.

Yan and He (1988) in their papers proved the influence of porous media capillarity on the dew pressure of a gas condensate system. They state that the retrograde condensation is accelerated in the porous media and there exists a movement into the higher pressure of the saturation curve compared to a flat surface case (Fig. 2).

A contrary conclusion is found in the work of Zhu and Huang (1988). The porous media dew pressure of the gas condensate in this paper is driven below the flat surface dew point and impact of the porous media in a near-critical condition was small. In the author's opinion the main part of their experimental work was done using conditions that satisfied the similarity-of-scale theorem. The probability of any capillarity effect in highly permeable rock is low.

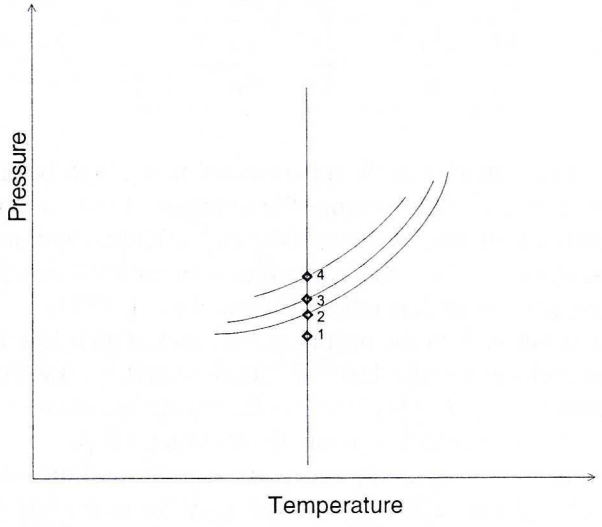

Fig. 2. Schematic impact of adsorption-capillary effects near phase boundary (dew curve)
1 — monolayer adsorption, 2 — multilayer adsorption, 3 — capillary condensation, 4 — bulk condensation

Rys. 2. Wpływ efektów kapilarno-adsorpcyjnych w pobliżu krzywej rosy
1 — adsorpcja jednowarstwowa, 2 — adsorpcja wielowarstwowa, 3 — kondensacja kapilana, 4 — kondensacja objętościowa

The simple comparison of the average porous radius of model sandstone rock using a modified Kozeny-Carman equation (Dullien 1992) is given in Table 1. It is evident (Defay, Prigogine 1966) that capillarity effects may be noticeable at a pore-radius of 10^{-5} cm. This condition limits the investigation area to porous rocks below $1 \cdot 10^{-3}$ μm^2 (1 mD). This is consistent in Lee's (1989) and Brusilovsky's (1990) work. The capillary effects observed by the Russian researches may be caused by accompanying laboratory effects.

TABLE I

The comparison of permeability of rock with average hydraulic porous radius using modified Cozeny-Karman equation. It was assumed 20% of effective porosity of rock

TABLICA I

Porównanie przepuszczalności ośrodka porowatego i średniego promienia porowego wyznaczonego równaniem Cozeny-Karmana dla założonej porowatości efektywnej 20%

k [μm^2]	r [10^{-8} m]
0.00001	6.3
0.0001	20
0.01	63
0.1	200
1	630
10	2000

Part of the experimental work was been performed using high-permeability porous media. The selection of sand or highly permeable sandstone ($250 \cdot 10^{-3}$ m^2 (250 mD)) as a PVT cell charge was not fortunate, because of the high effective hydraulic pore radius.

The manner of the dynamic fluid exchange process in the PVT cell during saturation pressure measurement is open to discussion (Sigmund et al. 1974).

The second open question is in the occurrence of rock with a low hydraulic radius (below 10 μm) in real rocks below the depth of 3000m with oil-wet wettability. This has been negated by Sigmund et al. (1974).The accompanying question is the existence of curvature systems ($<10^{-5}$ cm) with low connate saturation (S_{wi}).

In the opinion author of this paper the necessary condition of oil-wet characteristics for inclusion of a solid-gas interface interaction may be overcome for near-critical systems, when perfect condensate coverage is observed (see Wiliams, Dawe, 1989). The last opinion is confirmed by a recently published paper by Bertrand et al. (1999).

An excellent discussion about water- and oil-wet rock containing biogenic gas originating from the degeneration of organic matter by anaerobic organism's as well as about thermogenic gas from the biodegradation of liquid hydrocarbon is presented in papers by Debrandes and Bassiouni(1990) and Sassen (1988). In deep reservoirs below

3000 m (bsl) there exist possible conditions for the deposition of bitumen residuum and/or sulphur compounds which makes the porous environment an oil-wet system.

The experimental procedures regarding the capillarity effect in the laboratory: PVT experiments with cores are largely discussed in papers by Danesh et al. (1988). The authors conclude that all experiments performed in the past have a doubtful meaning. They emphase that high gravity effects, especially in the long horizontal core, during the equilibrium process totally camouflage the effects of capillarity. Similar conclusions about influence of gravity effects in near critical fluid may be found in the work of Wiliams and Dawe (1989). In their opinion there is no possible to perform satisfactory experiments on long horizontal cores with a gas condensate system in the laboratory.

The opinion of Lee (1989) and Guo (1996) confirm the necessity to include the capillary effects in the case of deep reservoirs with low permeability and oil-wet wettability.

3. Hydrocarbon adsorption phenomena in porous rocks near the saturation curve

The adsorption phenomena in porous media may have a significant impact on the reserve-distribution of oil and gas fields, coal-beds or geothermal reservoirs. Papers by Economides, Miller (1986) and Satik, Horne and Yortsos (1995) suggests the possibility to cover up to 85% of water reserves in the adsorption phase in vapour-dominated ($T > 300°C$) geothermal systems.

The adsorption process may largely be distinguished from surface adsorption observed in the chemical labs. The main two differentiating reasons are:

1) the existence of capillary condensation phenomena in the narrow pores,
2) the possibility of blocked flow access in the porous network.

The progress in the fundamentals of adsorption theory may be found in the Dąbrowski paper (2001). Unfortunately, many works describe single-component gas adsorption. The adsorption phenomena related to porous media have been presented in many textbooks (ie. Defay, Prigogine 1966; Reid, Modell 1974; Adamson 1990; Dullien 1992). Advances in the adsorption process in high-pressure porous media may be found in papers by Shapiro, Stenby (1996, 2000, 2001), Guo et al. (1996), Satik, Horne, Yortsos (1995), and Yortsos, Stubos (2001) .

The adsorption and capillary effects are complementary phenomena. In the areas where the interfacial surface tension is falling, a greater impact of adsorption forces may be observed (i.e. near critical point).

3.1. Simple adsorption models

In this paper two models of adsorption have been considered. Models describing of adsorption may be divided into two groups: the first group consisting of models of adsorption of single pore capillary or flat surface. In such cases no adsorption/desorption

hysteresis observed (Adamson 1990; Dąbrowski 2001). The second group is of models with adsorption/desorption in the pores. The classification of pore structure according to IUPAC is shown in the Table 2.

TABLE 2

Classification of pores according to the International Union of Pure and Applied Chemistry (IUPAC) (Everett 1972)

TABLICA 2

Klasyfikacja porów zgodna z ustaleniami International Un ion of Pure and Applied Chemistry (IUPAC) (Everett 1972)

	Pore width	Major process
Micropore	Less than 20 Å	Mono-layer adsorption and volume filling
Mesopore	Between 20 and 500 Å	Multi-layer adsorption and capillary condensation
Macropore	Larger than 500 Å	Multi-layer adsorption and capillary condensation

From the set of the known adsorption isotherm (Linear-Henry, Monolayer--Freundlich, Langmuir, Multilayer-BET, FHH) (Adamson 1990): the last (FHH — Frenkel-Halsey-Hill is most suitable for porous media. The derivation of this model has its origin in the potential adsorption theory (Polanyi). Using this form of adsorption, it is possible to express multi-component film adsorption in terms of simple, cylindrical capillarity (Adamson 1990; Satik, Horne, Yortsos 1995). Based upon the FHH adsorption model, the thickness of the adsorbed film may be computed:

$$t = \left(\frac{\varepsilon_0}{RT \ln \frac{p_v^{\infty}}{p_v}} \right)^{1/\alpha} \tag{1}$$

where;

t — thickness of adsorbed layer,
ε_0 — adsorption potential of the solid surface,
p_v^{∞} — vapor saturation pressure at flat surface,
p_v — actual vapor pressure,
α — empirical parameter (usually in the range 2–3).

This equation does not work at low pressures, but in this paper only high and moderate pressures are discussed.

There is no data suitable for performing the computation of multi-component hydrocarbon adsorption using this equation. There are some nitrogen, benzene, n-heptane,

water, methane, ethane, n-butane data (Hsieh et al. 1981; Shang et al. 1995; Shapiro, Stenby 1996). Because this paper principally concerns PVT-VLE capillary condensate, some simplification, based upon experimental observation, has been made.

According to Shang et al. (1995) the analysed values of film thickness are independent of the chemical nature of the adsorbent for most system at coverage greater than a mono-layer (i.e. for mega and mesopore structures). The set of adsorbed layer film thickness is shown in Table 3 and on Fig. 3. Example of methane adsorption in the Barea sandstone is shown on Fig. 4 (Hsieh et al., 1981). Alternatively de Boer et al. (1956) a simplified procedure for the critical film-thickness of the adsorption layer may be used with characteristic adsorption:

$$RT \ln\left(\frac{p_v}{p_v^{\infty}}\right) = \frac{\sigma V_L}{r - t_e}\left[\frac{t_e}{2 \cdot (r - t_e)} + 1\right] \tag{2}$$

where:

t_e — critical film thickness according to the de Boer and co-workers (Adamson 1990),
p_v^{∞} — vapor saturation pressure at flat surface,
p_v — actual vapour pressure,
r — capillary radius,
σ — interfacial surface tension,
V_L — liquid volume,
R — gas constant,
T — temperature.

The maximum thickness of adsorption film observed in the real mesopore system was 23 Å (Adamson 1990).

TABLE 3

The thickness of adsorption film in the mesopore structures (Shang et. al. 1995)
(p" — saturation pressure, p — gas phase pressure)

TABLICA 3

Grubość filmu warstwy adsorpcyjnej w mezoporach (Shang et. al. 1995)
(p" — ciśnienie nasycenia, p — ciśnienie fazy gazowej)

p/p"	t [Å]
0.5	5.9
0.6	6.5
0.7	7.4
0.8	8.6
0.9	12.7

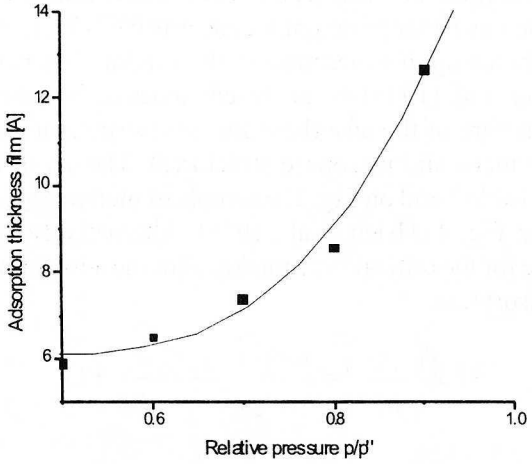

Fig. 3. Adsorption film thickness (t) for mega- and mesopore structure of tight rocks (based upon Shang et al. 1995 paper)
p" — saturation pressure, p — gas phase pressure

Rys. 3. Gdubość warstwy adsorpcyjnej dla mega- i mezoporów zwięzłych skał (na podstawie pracy Shang et al. 1995)
p" — ciśnienie nasycenia, p — ciśnienie fazy gazowej

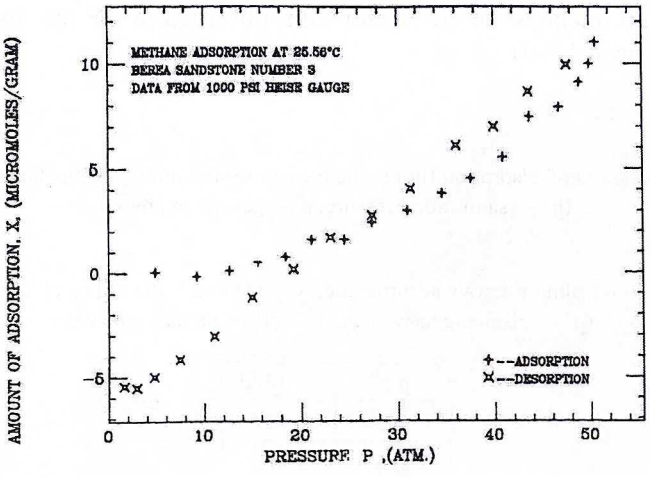

Fig. 4. High pressure isotherm of methane adsorption in the bare sandstone core example (Hsieh et al. 1981)

Rys. 4. Izoterma wysokociśnieniowej adsorpcji metanu w rdzeniu piaskowcowym (Hsieh et al. 1981)

3.2. Capillary condensation in the meso-pores of a porous media

The adsorption/desorption in the pores is closely connected with the capillary condensation process. The capillary condensation is modelled by various types of the Kelvin equation (Defay, Prigogine 1966; Adamson 1990; Al-Rub, Datta 1998).

The simplest form of equation is (Defay, Prigogine 1966):

$$\ln\left(\frac{p_v}{p_v^{\infty}}\right) = -\frac{2 \cdot \sigma \cdot V_L}{R \cdot T \cdot r} \tag{3}$$

A more convenient form is (Adamson 1990):

$$\ln\left(\frac{p_v}{p_v^{\infty}}\right) = -\frac{2 \cdot \sigma \cdot V_L}{R \cdot T \cdot (r - t)} \tag{4}$$

The above equation may be useful for mega- and mesopores. Parameter t is responsible for decreasing the capillary radius by the adsorption film.

A new multi-component form of Kelvin equation (SS-MKE) has been derived by Shapiro, Stenby (1997):

$$p_c = p_d \left[\frac{V_{gl}}{V_l} \ln\left(\frac{p_g}{p_d}\right) + \frac{p_g}{p_d} + 1\right] \tag{5}$$

where:

p_c — capillary pressure,

p_d — dew pressure for flat surface,

V_{gl} — mixed volume $V_{gl} = \sum_{i=1}^{nc} x_i^D V_i^G$,

x_i^D — composition of i-liquid component at dew pressure,

V_i^G — partial molar volume of vapour (gas) i-component.

This equation is valid only in the vicinity of the dew curve and fails in the critical--point area.

An extended Kelvin equation, which describes a falling single-component of vapour pressure in a curved environment (micropore structure) may take the form (Al-Rub, Datta 1998)

$$\ln\left(\frac{p_v}{p_v^{\infty}}\right) = C^E - \frac{\Delta H_{vl}^E}{RT} - \frac{2\sigma V_L}{rRT} \tag{6}$$

This equation differs from the traditional Kelvin equation for single component by excess enthalpy vaporisation $\left(\frac{\Delta H_{vl}^{E}}{RT}\right)$ and integration term (C^E). This equation is inconvenient to use in the present study, because is designed for very narrow pores (micropores).

The introduction of a different shape of capillary allows the hydraulic Kelvin radius to be generalised as:

$$r_h = \frac{r}{h_g + 1} \tag{7}$$

where h_g is a pore-shape generalisation factor using the approach adopted by Braunauer et al. (see Al-Rub, Datta 1998).

3.3. Capillary-adsorption vapour-liquid equilibrium (VLE) model

In the curved surface inside porous media for a stationary state of the second kind (based upon the Prigogine definition) following set of equations is valid (neglecting gravitational force):

$$p_v(T_v, \mu_1, \mu_2, ..., \mu_{nc}) - p_l(T_l, \mu_1, \mu_2, ..., \mu_{nc}) = \frac{2 \cdot \sigma(p_v, T_v, \mu_1, \mu_2, ..., \mu_{nc})}{r} \tag{8}$$

$$T_v = T_l \tag{9}$$

where T — temperature and μ_i — chemical potential of i-component, can be varied independently, and r is allowed to vary at the same time.

Based upon the set of equations (8)–(9) it is convenient to the write capillary--adsorption vapour-liquid equilibrium in porous media as the following equilibrium as a necessary condition for every component:

$$\mu_i^L = \mu_i^V = \mu_i^{Lad} = \mu_i^{Vad}; \quad i = 1, ..., n_c \tag{10}$$

where: $\mu_i^L, \mu_i^V, \mu_i^{Lad}, \mu_i^{Vad}$ — the chemical potential of the i-component adequately: free liquid, vapour, adsorption liquid, adsorption vapour.

At the dew point of capillary condensation phenomena three types of chemical potential exist:

$$\mu_i^L = \mu_i^V = \mu_i^{Vad}; \quad i = 1, ..., n_c \tag{11}$$

Using classical theory the following set of equations may be written:

Thermodynamic balance equation group:

$$f_i^L(p_v - p_c, T, x_1, x_2, \ldots, x_{nc}) - f_i^V(p_v, T, y_1, y_2, \ldots, y_{nc}) = 0; \quad i = 1, \ldots, n_c \tag{12}$$

Material balance equation group:

$$\sum_{i=1}^{nc} x_i - 1 = 0 \tag{13}$$

$$\sum_{i=1}^{nc} y_i - 1 = 0 \tag{14}$$

$$z_i - y_i = 0; \quad i = 1, \ldots, n_c \tag{15}$$

where z_i — overall i-component mole fraction ($y_i = z_i$ at dew point),

Laplace equation:

$$p_v - p_l - \frac{2 \cdot \sigma}{r_e} = 0 \tag{16}$$

Modified Kelvin equation:

$$\ln\left(\frac{p_v}{p_v^{\infty}}\right) = -\frac{2 \cdot \sigma \cdot V_L}{R \cdot T \cdot (r - t)} \tag{17}$$

Interfacial multi-component surface tension:

$$\sigma^{1/E} = \frac{p_v}{Z^v RT} \sum_{i=1}^{nc} \left[\left(\frac{Z^V}{Z^L}\right) \cdot x_i - y_i\right] \cdot \pi_i \tag{18}$$

where:

σ — interfacial surface tension (IFT) [N/m],
Z^v, Z^L — vapour and liquid phase compressibility factor [–],
E — an empirical dimensionless constant [–],
π_i — parachor of the i-component (Danesh 1991; Weinaug, Katz 1943) [–].

This set of nonlinear equations (11) may be modified by expanding them using the Taylor series (assuming that $p_v >> p_c$):

$$\mu_i^V(p_v,T,y_1,y_2,\ldots,y_{nc})=\mu_i^L(p_v-p_c(r,t),T,x_1,x_2,\ldots,x_{nc})= \tag{19}$$

$$=\mu_i^L(p_v,T,x_1,x_2,\ldots,x_{nc})+\frac{\partial\mu_i^L(p_v,T,x_1,x_2,\ldots,x_{nc})}{\partial(p_v-p_c)}p_c+$$

$$-\frac{\partial^2\mu_i^L(p_v,T,x_1,x_2,\ldots,x_{nc})}{\partial(p_v-p_c)^2}p_c^2+\ldots$$

Taking into consideration only the first term, the chemical potential of the *i*-component in the liquid phase may be calculated:

$$\mu_i^L(p_v-p_c(r,t),T,x_1,x_2,\ldots,x_{nc})= \tag{20}$$

$$=\mu_i^L(p_v,T,x_1,x_2,\ldots,x_{nc})-\frac{\partial\mu_i^L(p_v,T,x_1,x_2,\ldots,x_{nc})}{\partial(p_v-p_c)}p_c(r,t)$$

or using the fugacity of the i-component assuming isothermal conditions:

$$\ln f_i^L(p_L,T,x_1,x_2,\ldots,x_{nc})= \tag{21}$$

$$=\ln f_i^L(p_v,T,x_1,x_2,\ldots,x_{nc})-\frac{\partial\ln f_i^L(p_v,T,x_1,x_2,\ldots,x_{nc})}{\partial(p_v-p_c)}p_c$$

The derivative on the right side is a molar-partial component volume:

$$\frac{\partial\ln f_i^L(p_v,T,x_1,x_2,\ldots,x_{nc})}{\partial p_v}=\frac{\overline{V}_i^L}{RT} \tag{22}$$

or

$$\overline{V}_i=\left(\frac{\partial V}{\partial n_i}\right)_{T,p,n_{j\neq i}} \tag{23}$$

Equation (12) may be rewritten in the form:

$$\ln f_i^v(p_v,T,y_1,y_2,\ldots,y_{nc})=\ln f_i^L(p_v,T,x_1,x_2,\ldots,x_{nc})-\overline{V}_i^L\frac{p_c(r,t)}{RT} \tag{24}$$

where:

$\overline{V}_i^L$ — partial molar liquid component volume.

3.4. Difference between bulk and capillary condensation dew-point curve

Based upon the above derivation the difference between bulk and capillary condensate dew points (N_v = 1, where N — vapour phase mole fraction) the following equations may be formulated:

$$F(N_v = 1, p_c(r,t) = 0 \equiv 1 - \sum_{i=1}^{nc} \frac{z_i}{K_i} = 0 \tag{25}$$

$$F(N_v = 1, p_c(r,t) \neq 0 \equiv 1 - \sum_{i=1}^{nc} \frac{z_i}{K_i^{\infty}} \cdot \exp\left(- \int_0^{p_c(r,t)} \varepsilon_i dp \right) = 0 \tag{26}$$

where:

$\varepsilon_i = \dfrac{\overline{V}_i^L}{R \cdot T}$ — component Poynting factor,

or simplified

$$F(N_v = 1, p_c(r,t) \neq 0 \equiv 1 - \sum_{i=1}^{nc} \frac{z_i}{K_i^{\infty}} \cdot \exp\left(-\varepsilon_i p_c(r,t)\right) = 0 \tag{27}$$

3.5. Equilibrium constant modification for accountable capillary effects

Based upon equation (24) the new capillary condensation equilibrium constant may be introduced:

$$K_i = K_i^{\infty} \cdot \exp\left(\int_0^{p_c(r,t)} \varepsilon_i dp \right) \tag{28}$$

or after simplification based on constant partial molar volume:

$$K_i = K_i^{\infty} \cdot \exp\left(\varepsilon_i p_c(r,t)\right) \tag{29}$$

3.6. An algorithm for the calculation of the capillary condensation dew pressure

The proposed algorithm for calculation of the capillary condensation dew pressure consists of the following steps:

1. Compute set of initial equilibrium constants K_i^{∞}.

2. Compute thickness (t) of adsorption film using any meso-pores adsorption model (i.e. Frankel-Halsey-Hill, simplified de Boer et al., etc.).
3. Compute the interfacial tension (IFT) (σ) using scale or parachor model.
4. Compute capillary pressure p_c.
5. Compute the set of liquid partial volume of components $\overline{V}_i^L$ and Pointing factors (ε_i)
6. Compute new-corrected equilibrium constants using equation (29).
7. Compute the newly-corrected condensate capillary equilibrium composition of the liquid phase.
8. Perform saturation pressure correction for capillary/bulk vapour/liquid equilibria using (27).
9. Repeat steps 2–7 until convergence is reached.

3.7. Capillary modification for the Rachford-Rice equation

Based upon the new definition of capillary condensation equilibrium constant a new modification of the Rachford-Rice equation is proposed:

$$F(N_v) \equiv \sum_{i=1}^{nc} \frac{z_i\left(K_i^{\infty} \cdot \exp\left(\varepsilon_i p_c(r,t)\right)-1\right)}{N_v\left(K_i^{\infty} \cdot \exp\left(\varepsilon_i p_c(r,t)\right)-1\right)+1} = 0 \tag{30}$$

where:

N_v — the vapour phase faction.

3.8. Derivation of modified tangent plane criterion for capillary condensation (MTPCCC)

Below is a proposition to modification (by equation (39)) Michelsen (1982a) Gibbs tangent plane stability theory for capillary condensation.

The theory of the Gibbs (Michelsen, tangent plane 1982a) enables the verification of the thermodynamic state of the investigated phase (e.g. the initial phase) $z(z_1, z_2, \ldots, z_{nc})$. Let N moles of system be divided into two phases:

I. Firstly when $N - \varepsilon$.
II. Secondly with ε moles ($\varepsilon \to 0$).

Let one mole fraction of the original phase be designated as $y(y_1, y_2, \ldots, y_{nc})$. The change of Gibbs free energy in this case may be obtained using equation:

$$\Delta G \equiv G_I + G_{II} - G_0 = G(N-\varepsilon) + G(\varepsilon) - G_0 \tag{31}$$

where

$$G_0 = \sum_{i=1}^{nc} n_i \mu_i^0 \tag{32}$$

Gibbs free energy in the temperature T_0 and pressure p_0 for initial phase $z(z_1, z_2, \ldots, z_{nc})$.

The Gibbs free energy of I-phase may be calculated by expansion of the n-variables function to the Taylor series and truncation terms being higher than the first:

$$G(N-\varepsilon)=G(N)+\sum_{i=1}^{nc}\left(\frac{\partial G}{\partial n_i}\right)_N (N\cdot z_i-\varepsilon\cdot y_i) \tag{33}$$

By using the Gibbs-Duhem equation and because $G(N) = G_0$ above equation may be formed:

$$\Delta G=G_0-\varepsilon\sum_{i=1}^{nc}\left(\frac{\partial G}{\partial n_i}\right)_N y_i+(G)\varepsilon-G_0 \tag{34}$$

or by introducing the chemical potential:

$$\Delta G=\varepsilon\sum_{i=1}^{nc} y_i\cdot\mu_i(\boldsymbol{y})-\varepsilon\sum_{i=1}^{nc} z_i\cdot\mu_i(\boldsymbol{z}) \tag{35}$$

The thermodynamic stability of phase $z(z_1, z_2, \ldots, z_{nc})$ is equivalent to reaching the absolute minimum of Gibbs free energy in the system. This condition may be expressed as inequality:

$$F(\boldsymbol{y})\equiv\sum_{i=1}^{nc} y_i\cdot[\mu_i(\boldsymbol{y})-\mu_i(\boldsymbol{z})]\geq 0 \tag{36}$$

for all composition data of the originating phase $\boldsymbol{y}(y_1, y_2, \ldots, y_{nc})$

Stability requires that the tangent plane at no point lies above the surface of the Gibbs free energy of the initial phase $z(z_1, z_2, \ldots, z_{nc})$. Stability condition of equation (36) is tested at stationary points:

$$\left(\frac{\partial F}{\partial y_i}\right)_N\equiv\mu_i(\boldsymbol{y})-\mu^0{}_i(\boldsymbol{z})-F(\boldsymbol{y})=0 \tag{37}$$

or by using fugacity coefficients for the bulk liquid phase:

$$\ln Y_i+\ln\phi_i(\boldsymbol{y})-\ln z_i-\ln\phi_i(\boldsymbol{z})-\ln\phi_i(\boldsymbol{z})=0;,\quad i=1,\ldots,nc \tag{38}$$

or for capillary condensation liquid phase using equation (28):

$$\ln Y_i+\ln\phi_i(\boldsymbol{y})^{\infty}-\ln z_i-\ln\phi_i(\boldsymbol{z})^{\infty}+\frac{\overline{V}_i^L}{RT}p_c=0;\quad i=1,\ldots,nc \tag{39}$$

where

$$Y_i=y_i\exp(-K);\ (K\text{ — }\textit{non negative number}) \tag{40}$$

and mole fraction of the originating phase:

$$y_i = \frac{Y_i}{\sum_{i=1}^{nc} Y_i} \tag{41}$$

For instability of the initial phase $z(z_1, z_2, \ldots, z_{nc})$ one may test using the verification of inequality:

$$\sum_{i=1}^{nc} Y_j \leq 1 \quad \textit{for stable system} \tag{42}$$

$$\sum_{i=1}^{nc} Y_j > 1 \quad \textit{for unstable system} \tag{43}$$

at all stationary points.

This scheme differs from the traditional Michelsen algorithm (1982a) by introducing a new equilibrium for stationary points in equation (38), which is estimated from equation (28).

Use of this proposed stability test allows computation of the vapor/liquid equilibrium in the capillary condensation area without the necessity to compute the saturation pressure of flat and curved systems. A similar approach — use of tangent plane theory instead computation of saturation pressure — has been applied into the multiphase isenthalpic algorithm (Nagy 1992a, 1992b) and during isothermally constant volume depletion modelling of gas condensate systems (e.i. Nagy 1996).

4. Application of theory to possible reservoir gas-condensate systems

4.1. Selection of a Cubic Equation of State (CEOS)

The computation in this work has been done using a new version of the Peng-Robinson equation. From among many versions of PR CEOS the Tsai and Chen (1998) and Magoulos, Stamataki (1990) versions has been chosen. In the selection of CEOS the following criteria have been considered:

- versatility in whole temperature and pressure for light hydrocarbons (C_1–C_6),
- versatility in whole temperature and pressure for light hydrocarbons (C_7–C_{30}),
- accuracy of density of each phase,
- accuracy of fugacity of each component in both vapour and liquid phase,
- accuracy of molar partial volume of every component in the liquid phase.

On the basis of several papers (Peng-Robinson 1976; Peneloux, Rauzy, Freze 1982; Stryjek, Vera 1986; Yu, Lu 1987; Firoozabadi 1988; Patel, Teja 1982; Siemek et al. 1987; Martin 1979; Soave 1972; Voros, Stamataki, Tassios 1994; Stamataki, Magoulos

2001) a new generation modified cubic equation-of-state based upon a translated Peng-Robinson form has been evolved. The first selected EOS is, in the opinion of the author, the most versatile cubic equation for polar and non-polar compounds. The second is simpler, because of the use only of the critical parameters of individual components.

The original Tsai and Chen (1998) and Magoulos, Stamataki (1990) form of the equation is given below:

$$p = \frac{RT}{v + t - b} - \frac{a}{(v + t)(v + t + b) + b(v + t - b)} \tag{44}$$

where t-the translated volume parameter, with which the volume calculated by the CEOS approaches the experimental value:

$$v_{exp} = v_{CEOS} + t \tag{45}$$

$$a = 0.45724 \frac{R^2 T_c^2}{p_c} \alpha(T) \tag{46}$$

$$b = 0.07780 \frac{RT_c}{p_c} \tag{47}$$

For this equation the following function of $\alpha(T)$ for Tsai and Chen (1998) has formed:

$$\alpha(T) = [1 + M(\omega)(1 - T_R) + N(1 - T_R)(0.7 - T_R)]^2 \tag{48}$$

where $M(\omega)$ and N are two parameters for each pure fluid. The $M(\omega)$ has following form:

$$M(\omega) = 0.20473 + 0.83548 \cdot \omega - 0.18470 \cdot \omega^2 + 0.16675 \cdot \omega^3 - 0.09881 \cdot \omega^4 \tag{49}$$

The value of N is calculated for each pure component. For the $\alpha(T)$ in the Magoulos, Stamataki (1990) form of EOS the standard Peng-Robinson Function is used.

The t-translated volume parameter for Tsai, Chen (1998) version of CEOS is computed from the equation:

$$t = \frac{RT_c}{p_c} [k_1 + k_2 (1 - T_R^{2/3}) + k_3 (1 - T_R^{2/3})^2] \tag{50}$$

where parameters k_1 and k_2 have following form:

$$k_1 = 0.00185 + 0.00438 \cdot \omega + 0.36322 \cdot \omega^2 - 0.90831 \cdot \omega^3 + 0.55885 \cdot \omega^4 \tag{51}$$

$$k_2 = -0.00542 - 0.51112 \cdot k_3 + 0.04533 \cdot k_3^2 + 0.07447 \cdot k_3^3 - 0.03831 \cdot k_3^4 \tag{52}$$

and where the k_3 — parameter has a specific value for every component. The important parametres N and k_3 are shown in the Table 4.

For the Stamataki and Magoulas (1990) equation of state a generalised form of the t-translated volume parameter function is used:

$$t = t_0 - (t_c - t_0)\exp\lambda\left|1 - \frac{T}{T_c}\right| \tag{53}$$

where

$$t_0 = \frac{RT_c}{p_c}[-0.014471 + 0.067498 \cdot \omega - 0.084862 \cdot \omega^2 + \\ + 0.067298 \cdot \omega^3 - 0.017366 \cdot \omega^4] \tag{54}$$

$$t_c = \frac{RT_c}{p_c}(03074 - Z_c) \tag{55}$$

$$\lambda = -10.2447 - 28.6312 \cdot \omega \tag{56}$$

$$Z_c = 0.0289 - 0.0701 \cdot \omega - 0.207 \cdot \omega^2 \tag{57}$$

The fugacity coefficient of the both CEOS is:

$$\ln\phi = (Z + C - 1) - \ln(Z + C - B) - \frac{A}{2\sqrt{2B}}\ln\left[\frac{Z + C + (1+\sqrt{2})B}{Z + C + (1-\sqrt{2})B}\right] \tag{58}$$

where

$$A = \frac{ap}{R^2T^2} \tag{59}$$

$$B = \frac{bp}{RT} \tag{60}$$

$$C = \frac{tp}{RT} \tag{61}$$

$$Z = \frac{pv}{RT} \tag{62}$$

The dimensionless form of above CEOS is as follows:

$$Z^3 + (-1 + B + 3C) \cdot Z^2 + (3C^2 - 3B^2 - 2C - 2CB + A) \cdot Z + \tag{63}$$

$$-C^2 - 2CB + B^2 + C^2B + AC - AB + C^3 - 3CB^2 + B^3 = 0$$

For this equation classical mixing rules for CEOS are recommended:

$$a = \sum_{i=1}^{n} \sum_{k=1}^{n} \xi_i \xi_k (1 - k_{ik}) \sqrt{a_i a_k} \tag{64}$$

$$b = \sum_{i=1}^{n} \xi_i b_i \tag{65}$$

where ξ_i — molar liquid or vapor composition of the i-component and the k_{ij} — binary interaction coefficient (BIC) is obtained from experimental binary VLE data or adopted from generalised correlations. In this work the set of BIC's from Kordas et al. (1995), Arabi and Firoozabadi (1995) or Soereide and Whitson(1990) has been selected, but the last two correlations were preferred.

The parameters of N and k_3 are not listed for the heavy fraction, so for mixtures with C_{11}–C_{20} pseudo-components only the Magoulos and Stamataki form is used.

The fugacity coefficient of the i-component in the phase is calculated from the following equation (in the original Tsai and Chen (1998) paper this equation was written completely erroneously):

TABLE 4

Selected hydrocarbon and non-hydrocarbon component constants needed to be used with Tsai-Chen (1998) VTPRCEOS. Other critical parameters have been chosen from Reid, Prausnitz, Polling (1987)

TABLICA 4

Wybrane stałe składników węglowodorowych i niewęglowodorowych gazu ziemnego i ropy naftowej dla równania VTPR Tsai-Chen(1998). Inne własności w oparciu pracę Reid, Prausnitz, Polling (1987)

	Name	N	k_3
1	methane	0.08248	0.20978
2	ethane	0.11292	0.22277
3	propane	0.16846	0.22685
4	i-butane	0.18381	0.25559
5	n-butane	0.15546	0.2537
6	i-pentane	0.14908	0.2764
7	n-pentane	0.16851	0.26392
8	n-hexane	0.16397	0.27558
9	n-heptane	0.17822	0.26154
10	n-octane	0.19773	0.24145
12	n-decane	0.25192	0.13471
13	CO_2	0.11333	0.28996
15	N_2	0.09967	0.24086

$$\ln\phi_i = \frac{b_i}{B}(Z+C-1) - \ln(Z+C-B) - \frac{A}{2\sqrt{2}\cdot B}\left[\frac{2\sum_{i=1}^{nc}\xi_j a_{ij}}{A} - \frac{b_i}{B}\right] \cdot \tag{66}$$

$$\cdot \ln\left[\frac{Z+C+(1+\sqrt{2})B}{Z+C+(1-\sqrt{2})B}\right]$$

where:

ξ_i — molar liquid or vapour composition of the i-component.

4.2. Accuracy of computation of dew curve tested on flat surface VLE data

Accuracy of computation of VLE using VT PR CEOS has been tested on the Hoffman et al. experimental data (1953). The set of experimental data includes a high content of heavy hydrocarbons (30%). For this mixture a special procedure of splitting the heavy hydrocarbon (C_{7+}) fraction into a set of pseudo-components pC_7–pC_{20+} using the classical triple probability parameter Whitson model (1983). Detailed of grouping procedure may be found in Ahmed (1985, 1989) and Pedersen et al. (1982, 1989a,

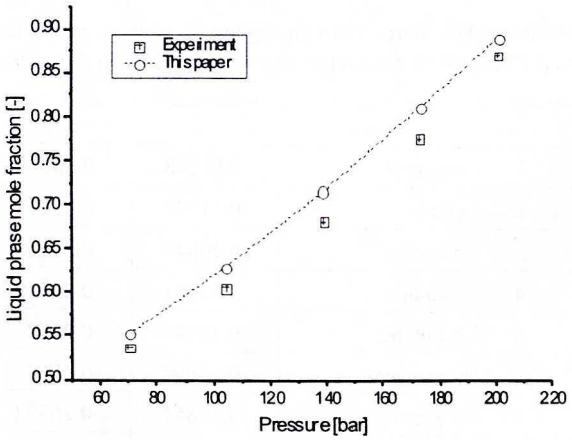

Fig. 5. Comparison of computation of liquid mole phase fraction with experimental data (Hoffman et al. 1953) using VT PR EOS with splitting procedure of Whitson with generalized BIC correlation of Pedersen (1989)

Rys. 5. Porównanie obliczenia udziału molowego fazy ciekłej z danymi eksperymentalnymi (Hoffman et al. 1953) obliczonymi równaniem VTPR z danymi oddziaływania binarnego według Pedersena (1989) przy zastosowaniu metody rozdziału frakcji C_{7+} według Whitsona

TABLE 5

Original composition of Hoffman et al. (1953) mixture

TABLICA 5

Skład roztworu nr 2 według Hoffmana et al. (1953)

Component	% mole
methane	52.00
ethane	3.81
propane	2.37
n-butane	0.96
i-butane	0.76
n-pentane	0.51
i-pentane	0.69
hexane	2.06
heptane plus	36.84

1989b, 1996), Behrens and Sandler (1986), as well as in Whitson papers (1983, 1985a, 1985b). The critical parameters of the pseudo-fractions has been evaluated using Win (1957), Sim and Daubert (1980), Razi and Daubert (1980) correlations. The accuracy of computation of the liquid mole fraction is presented in Fig. 5. The composition mixture — original and modified is presented in Table 5 and 6. The comparison of computation results and experiments data is shown in the Table 9.

4.3. Interfacial tension at a high VLE pressure

The most important parameter needed in this algorithm is the proper evaluation of surface tension oil/condensate-gas in the high pressure VLE. The suggested is related to new papers Fanchi (1990), Danesh et al. (1991). Data from these papers has been used in the computations (Table 7). Verification of calculations has been tested using Firoozabadi et al. (1988) data. Comparison of computation is shown in Table 8. Average percentage deviation between measured and computed interfacial surface tension (IFT) is 4.62%.

4.4. A novel algorithm for describing capillary effects in the traditional VLE computation

Proposed steps in calculating reservoir equilibrium parameters:

1. Compute thickness of adsorption film using any meso-pores adsorption model.
2. Compute the interfacial tension (IFT) using scale or parachor model.
3. Compute the set of liquid partial volume of components $\overline{V}_i^L$.
4. Compute new-corrected equilibrium constants.

TABLE 6

Mixture 2 composition (Hoffman et al. 1953) with splitting pseudo-fraction according to Whitson procedure into pC_7–pC_{20+} pseudo-components, equilibrium constants and vapour phase composition at the flat surface bubble-point (230 bar, 366 K)

TABLICA 6

Skład roztworu 2 (Hoffman et al. 1953) z rozbiciem na pseudofrakcje zgodnie z procedurą Whitsona, stałe równowagi oraz skład fazu gazowej przy ciśnieniu pęcherzyków (dla powierzchni płaskiej) (230 bar, 366 K)

	Initial comp. z_i	Equilibrium constant K_i	Liquid phase comp. x_i
methane	0.519950	4.054299	0.926420
ethane	0.038096	0.648934	0.033284
propane	0.023698	0.200058	0.013528
i-butane	0.007599	0.088714	0.003277
n-butane	0.009599	0.067794	0.003620
i-pentane	0.006899	0.031106	0.001945
n-pentane	0.005100	0.025351	0.001312
n-hexane	0.020598	0.010184	0.003722
pC_7	0.026297	0.003446	0.002800
pC_8	0.023398	0.002320	0.002114
pC_9	0.023498	0.000871	0.001404
pC_{10}	0.026297	0.000712	0.001441
pC_{11}	0.042196	0.000389	0.001778
pC_{12}	0.039996	0.000191	0.001231
pC_{13}	0.036096	9.47E-05	0.000809
pC_{14}	0.031897	4.73E-05	0.000518
pC_{15}	0.027797	2.38E-05	0.000326
pC_{16}	0.024098	1.2E-05	0.000202
pC_{17}	0.020798	6.07E-06	0.000124
pC_{18}	0.017798	3.07E-06	7.48E-05
pC_{19}	0.015298	1.55E-06	4.47E-05
pC_{20+}	0.012999	7.83E-07	2.61E-05

TABLE 7

Composition of crude oil mixture used to verification of computations of surface tension (Firoozabadi et al. 1988)

TABLICA 7

Skład roztworu ropy naftowej użyty do obliczeń napięcia powierzchniowego (Firoozabadi et al. 1988)

Component	%mole
N_2	0.03
CO_2	2.02
C_1	51.53
C_2	8.07
C_3	5.04
i-C_4	0.83
n-C_4	2.04
i-C_5	0.84
n-C_5	1.05
C_6	1.38
C_{7+}	27.17

TABLE 8

Comparison of computation of surface tension based upon composition listed in table 5 (Firoozabadi et al. 1988)

TABLICA 8

Porównanie obliczeń napięcia powierzchniowego na podstawie składu z tablicy 5 (Firoozabadi et al. 1988)

Pressure [bar]	Measured [mN/m]	Calculated [mN/m]	% Dev
263	1.3	1.39	6.92
228.5	2.3	2.15	–6.52
194	3.3	3.17	–3.94
159.6	4.6	4.55	–1.09
Av. % Dev			4.62

5. Compute new-corrected condensate capillary equilibrium composition of liquid and vapour phases.
6. Compute set of initial equilibrium constants K_i^{∞} based upon the Wilson equation.
7. Perform capillary condensation stability tangent plane criterion (CCSTP).
8. Perform capillary/bulk VLE computation.

TABLE 9

Comparison of computation of liquid mole fraction of Hoffman mixture using VT PR EOS

TABLICA 9

Porównanie obliczeń udziału molowego fazy ciekłej roztworu Hoffmana według równania VTPR

Pressure [bar]	Experiment	This paper	% Dev
201.1	0.870	0.890	2.30
173.3	0.775	0.810	4.52
138.9	0.681	0.715	4.99
104.4	0.606	0.650	7.26
70.0	0.537	0.552	2.79
Average %Dev.			4.37

TABLE 10

Initial composition, equilibrium constants and liquid phase composition at the flat surface at 169 bar and 473 K of mixture 1

TABLICA 10

Początkowy skład, stałe równowagi i skład fazy ciekłej roztworu nr 1 przy ciśnieniu 169 bar (dla powierzchni płaskiej) i w temperaturze 473K

Component	Initial comp. z_i	Equilibrium constant K_i	Liquid phase comp. x_i
methane	0.6687	11.17221	0.517298
ethane	0.0686	3.780866	0.062846
propane	0.0395	1.572289	0.040886
i-butane	0.0073	0.833021	0.008255
n-butane	0.0182	0.696697	0.021261
i-pentane	0.0083	0.386658	0.010597
n-pentane	0.0103	0.339484	0.013441
n-hexane	0.0140	0.171896	0.020352
n-heptane	0.0100	0.093877	0.016094
n-octane	0.0100	0.052304	0.017775
n-nonane	0.0100	0.030234	0.019604
n-decane	0.1041	0.017567	0.224876
CO_2	0.0298	7.404272	0.025890
N_2	0.0012	19.49953	0.000826

4.5. Examples of influence of capillary-adsorption effects on the gas condensate system

In the Tables 10, 6, 12 are shown composition of mixtures 1, 2, 3 (respectively).

The impact of capillary — adsorption effects on equilibrium constants near near phase boundary of mixture 1 is presented in the Table 11. The computed interfacial tension of mixture 2 and 3 near phase boundary is given in the Tables 13 and 14.

The Figs. 6–32 show examples of the impact of adsorption-capillary effects. The capillary-adsorption impact on the vapour phase fraction near the flat-surface dew point (169 bar, 473 K) of mixture 1. In Fig. 5 are shown the effect of pore radius on the capillary pressure near phase boundary, near-flat surface dew point (169 bar, 473 K) of mixture 1. The Impact of pore radius on liquid density near the phase boundary near-flat surface dew point (169 bar, 473 K) of mixture 1 is shown in Fig. 6. In Fig. 7 is shown the influence of effective pore radius on bubble point movement. The flat--surface bubble pressure is estimated as 230 bar (at 366 K), capillary bubble pressure ($r_e = 5 \cdot 10^{-9}$ m) 201 bar for mixture 2 (Hoffman et al. 1953).

TABLE 11

Impact of capillarity-adsorption effects on equilibrium constants near phase boundary (flat surface) of mixture 1 (169 bar, 473 K)

TABLICA 11

Wpływ efektów kapilarno-adsorpcyjnych na stan w pobliżu krzywej nasycenia dla roztworu nr 1 przy ciśnieniu 169 bar (dla powierzchni płaskiej) i w temperaturze 473 K

Component	Average effective pore radius [m]			
	∞	$2 \cdot 10^{-08}$	$1 \cdot 10^{-08}$	$5 \cdot 10^{-09}$
methane	1.290821	1.301259	1.294868	1.259396
ethane	1.090972	1.09324	1.089763	1.073761
propane	0.966319	0.963972	0.961902	0.955964
i-butane	0.885045	0.879883	0.878505	0.878014
n-butane	0.856943	0.851041	0.850071	0.851998
i-pentane	0.784588	0.776524	0.776104	0.782313
n-pentane	0.767783	0.759301	0.759052	0.766378
n-hexane	0.68989	0.679415	0.679653	0.690861
n-heptane	0.623767	0.611921	0.612576	0.626825
n-octane	0.565349	0.552441	0.553334	0.569575
n-nonane	0.513219	0.49961	0.50073	0.518602
n-decane	0.466331	0.452195	0.453408	0.472159
CO_2	1.150086	1.155007	1.151106	1.130984
N_2	1.450216	1.467671	1.458349	1.404479

TABLE 12

Composition of the mixture no. 3

TABLICA 12

Początkowy skład roztworu nr 3

methane	0.7643
ethane	0.0746
propane	0.0312
i-butane	0.0059
n-butane	0.0121
i-pentane	0.005
n-pentane	0.0059
n-hexane	0.0079
n-heptane	0.01
n-octane	0.01
n-nonane	0.01
n-decane	0.037
CO_2	0.0249
N_2	0.0012

TABLE 13

Computed interfacial tension of mixture 2 near phase boundary (at temperature 366 K)

TABLICA 13

Obliczone napięcie powierzchniowe roztworu nr 2 w pobliżu krzywej nasycenia (w temp. 366 K)

Pressure [bar]	169	150	120	90
IFT [mN/m]	0.047	0.269	0.933	1.966

TABLE 14

Computed interfacial tension of mixture 3 near phase boundary (at temperature 473 K)

TABLICA 14

Obliczone napięcie powierzchniowe roztworu nr 3 w pobliżu krzywej nasycenia (w temp. 473 K)

Pressure [bar]	200	150	100	70	50
IFT [mN/m]	0.759	2.039	4.079	5.732	7.041

The change of capillary pressure is presented in Fig. 8. In Fig. 9 may be seen the influence of the effective pore radius on the liquid phase density near saturation phase boundary of mixture 2. The impact of effective pore radius on the vapour phase fraction at 60 bar below saturation pressure (173.4 bar at temperature 402 K) of mixture 2 is shown in Fig. 10, and capillary pressure in Fig. 11. Fig. 12 presents the influence of effective pore radius on the liquid phase density at 60 bar below saturation pressure of mixture 2. The change of saturation curve in the presence of a curvature of the porous media in mixture 2 (T = 366.6 K) is shown in Fig. 13. The next Fig. 14, presents the depression of the bubble point pressure versus curvature for mixture 2 (T = 366.6 K). Analysis of component-composition of the system in the vapour phase may be performed using Figs.15–16. Fig. 17 shows the change of methane content in the vapour phase as a function of pore radius for mixture 2 (366.6 K, 210 bar (flat surface)). Change of the intermediated component fraction in the vapour phase as a function of the pore radius for mixture 2 (366.6 K, 210 bar (flat surface)) is presented in Fig. 18, and change in the pseudo-decane fraction in the vapour phase is a function of pore radius for mixture 2—cf. Fig. 19. The most heavy pC_{20+} component-change of fraction in the vapour phase as a function of pore radius for mixture 2 may be seen in Fig. 20. Change of liquid composition is shown in Figs. 21–22. Fig. 23 presents the change of methane content in the liquid phase as a function of the pore radius for mixture 2, and Fig. 24 shows change of intermediate components. Change of pC_{10} and pC_{20+} component-content in the liquid phase is shown in Fig. 25. Mixture 3 represents the gas condensate system.

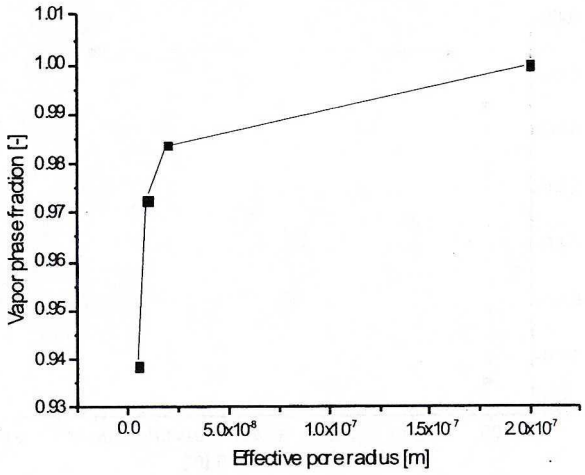

Fig. 6. Capillary-adsorption impact on the vapor phase fraction near flat surface dew point (169 bar, 473 K) of mixture 1

Rys. 6. Wpływ efektów kapilarno-adsorpcyjnych na udział fazy gazowej w pobliżu krzywej rosy (dla powierzchni płaskiej) dla roztworu nr 1(169 bar, 473 K)

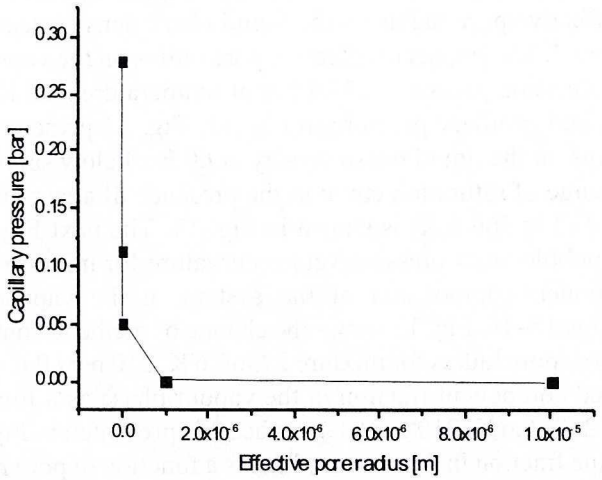

Fig. 7. Impact of pore radius on capillary pressure near phase boundary — near flat surface dew point (169 bar, 473 K) of mixture 1

Rys. 7. Wpływ promienia porowego na ciśnienie kapilarne w pobliżu krzywej rosy (dla powierzchni płaskiej) dla roztworu nr 1(169 bar, 473 K)

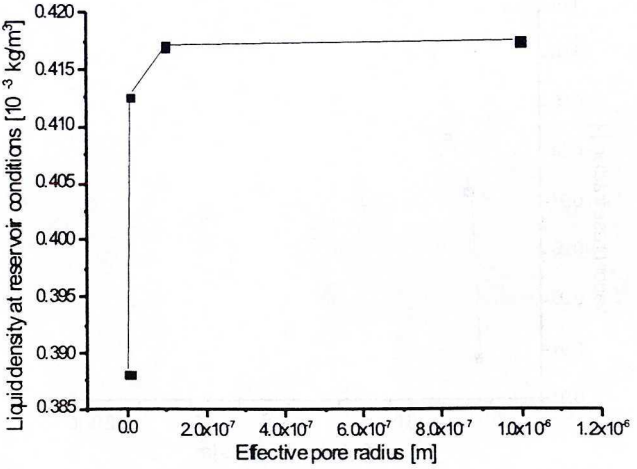

Fig. 8. Impact of pore radius on liquid density near phase boundary — near flat surface dew point (169 bar, 473 K) of mixture 1

Rys. 8. Wpływ promienia porowego na gęstość fazy ciekłej w pobliżu krzywej rosy (dla powierzchni płaskiej) dla roztworu nr 1(169 bar, 473 K)

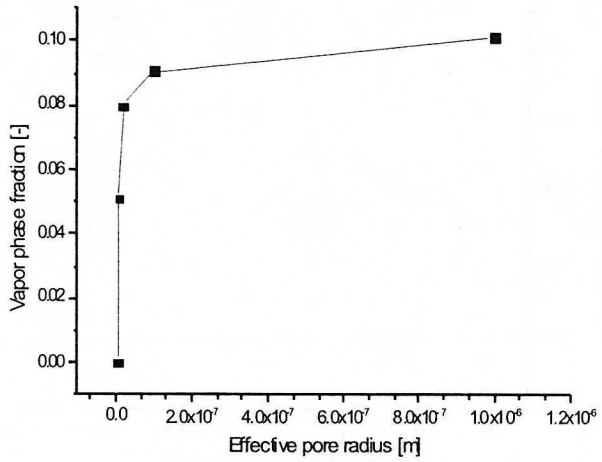

Fig. 9. Impact of effective pore radius on bubble point movement. Flat surface bubble pressure 230 bar, capillary bubble pressure ($re = 5 \cdot 10^{-9}$ m) 201 bar (at 366.6 K) of mixture 2

Rys. 9. Wpływ efektywnego promienia porowego na przesunięcie punktu pęcherzyków. Ciśnienie nasycenia (pęcherzyków) 230 bar, ciśnienia nasycenie (pęcherzyków) dla powierzchni zakrzywionej ($re = 5 \cdot 10^{-9}$ m) 201 bar (at 366,6 K) dla roztworu nr 2 (Hoffman et al. 1953)

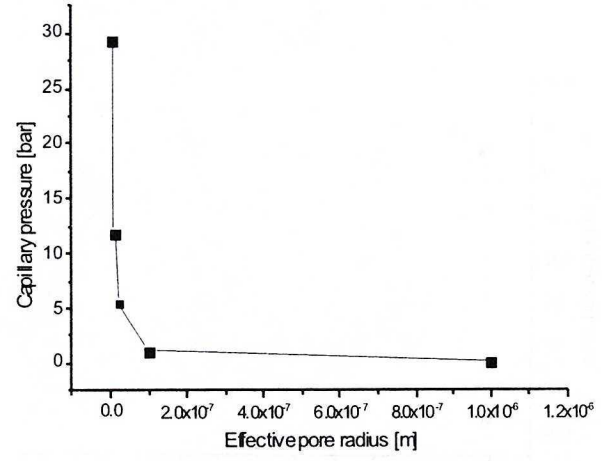

Fig. 10. Impact of effective pore radius on capillary pressure near saturation phase boundary. Flat surface bubble pressure 230 bar, capillary bubble pressure ($re = 5 \cdot 10^{-9}$ m) 201 bar (at 366.6 K) of mixture 2 (Hoffman et al. 1953)

Rys. 10. Wpływ efektywnego promienia porowego na ciśnienie kapilarne w pobliżu krzywej nasycenia. Ciśnienie nasycenia (pęcherzyków) 230 bar, ciśnienia nasycenie (pęcherzyków) dla powierzchni zakrzywionej ($re = 5 \cdot 10^{-9}$ m) 201 bar (at 366,6 K) dla roztworu nr 2 (Hoffman et al. 1953)

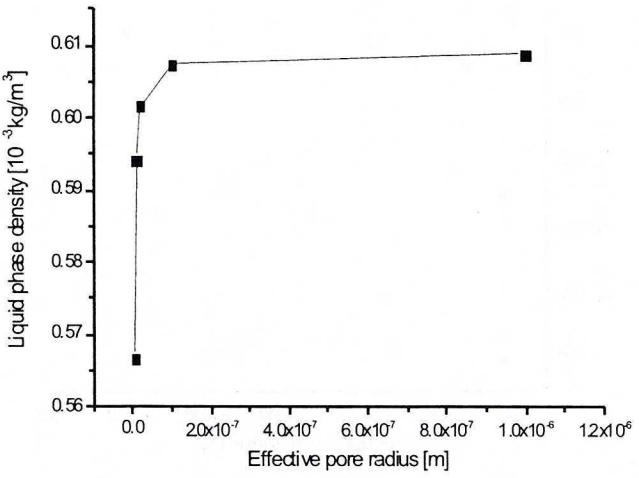

Fig. 11. Impact of effective pore radius on liquid phase density near saturation phase boundary. Flat surface bubble pressure 230 bar, capillary bubble pressure ($re = 5 \cdot 10^{-9}$ m) 201 bar (at 366.6 K) of mixture 2

Rys. 11. Wpływ efektywnego promienia porowego na gęstość fazy ciekłej w pobliżu krzywej nasycenia. Ciśnienie nasycenia (pęcherzyków) 230 bar, ciśnienie nasycenia (pęcherzyków) dla powierzchni zakrzywionej ($re = 5 \cdot 10^{-9}$ m) 201 bar (at 366,6 K) dla roztworu nr 2 (Hoffman et al. 1953)

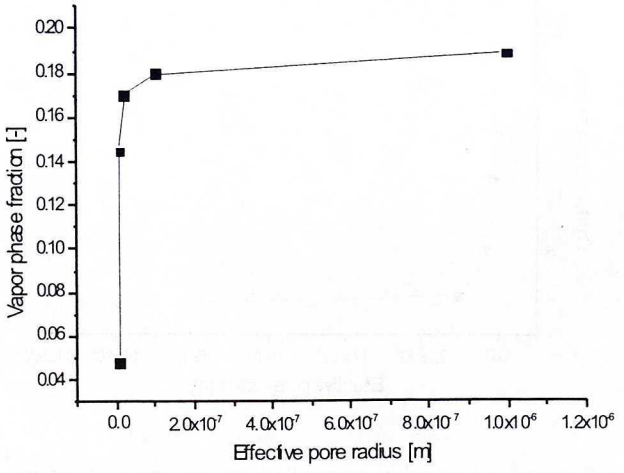

Fig. 12. Impact of effective pore radius on vapor phase fraction 60 bar below saturation pressure (173.4 bar at temperature 366.6 K) of mixture 2

Rys. 12. Wpływ efektywnego promienia porowego na udział fazy gazowej 60 bar poniżej krzywej nasycenia (p = 173.4 bar, T = 366,6 K) dla roztworu nr 2 (Hoffman et al. 1953)

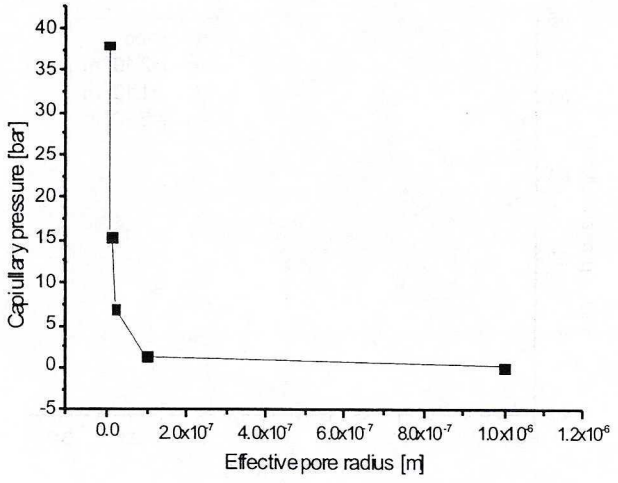

Fig. 13. Impact of effective pore radius on capillary pressure 60 bar below saturation pressure (173.4 bar at temperature 366.6 K) of mixture 2

Rys. 13. Wpływ efektywnego promienia porowego na ciśnienie kapilarne 60 bar poniżej krzywej nasycenia (p = 173.4 bar, T = 366,6 K) dla roztworu nr 2 (Hoffman et al. 1953)

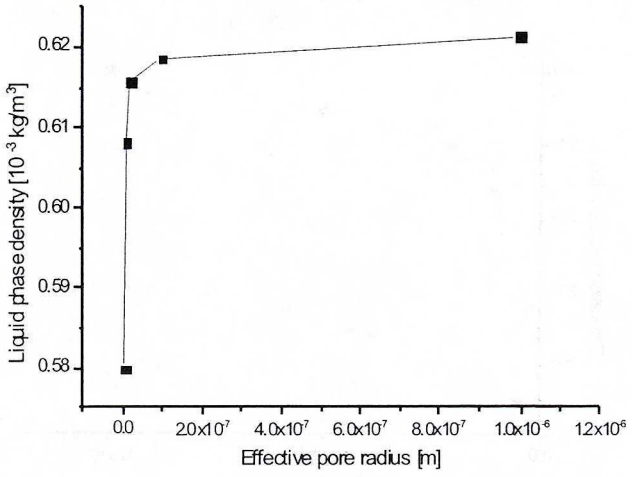

Fig. 14. Impact of effective pore radius on liquid phase density 60 bar below saturation pressure (173.4 bar at temperature 366.6 K) of mixture 2

Rys. 14. Wpływ efektywnego promienia porowego na gęstość fazy ciekłej 60 bar poniżej krzywej nasycenia (p = 173.4 bar, T = 366,6 K) dla roztworu nr 2 (Hoffman et al. 1953)

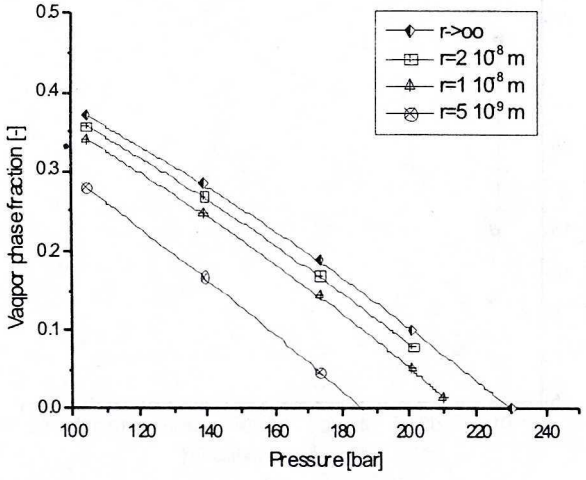

Fig. 15. The change of saturation curve in presence of curvature of porous media in the mixture 2 (T = 366.6 K)

Rys. 15. Zmiana krzywej nasycenia w obecności krzywizny ośrodka porowatego dla roztworu nr 2 (T = 366,6 K)

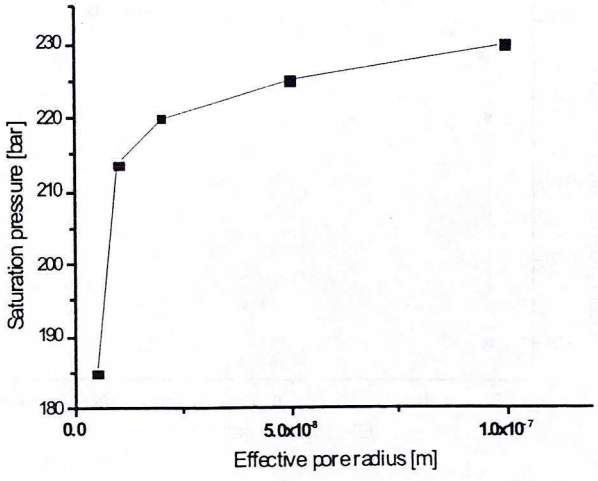

Fig. 16. Depression of bubble point pressure versus curvature for the mixture 2 (T = 366.6 K)

Rys. 16. Obniżenie ciśnienia nasycenia (pęcherzyków) w obecności krzywizny ośrodka porowatego dla roztworu nr 2 (T = 366,6 K)

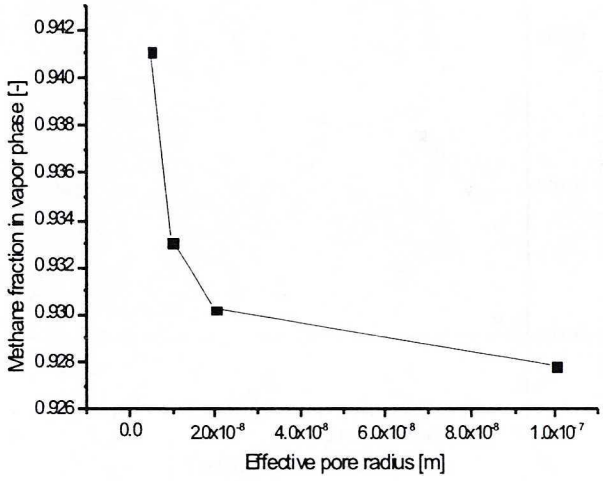

Fig. 17. Change of methane content in the vapor phase as a function of pore radius for the mixture 2 (366.6 K, 210 bar — flat surface)

Rys. 17. Zmiana zawartości metanu w fazie parowej jako funkcja promienia porowego dla roztworu 2 (366,6 K, 210 bar — dla fazy gazowej)

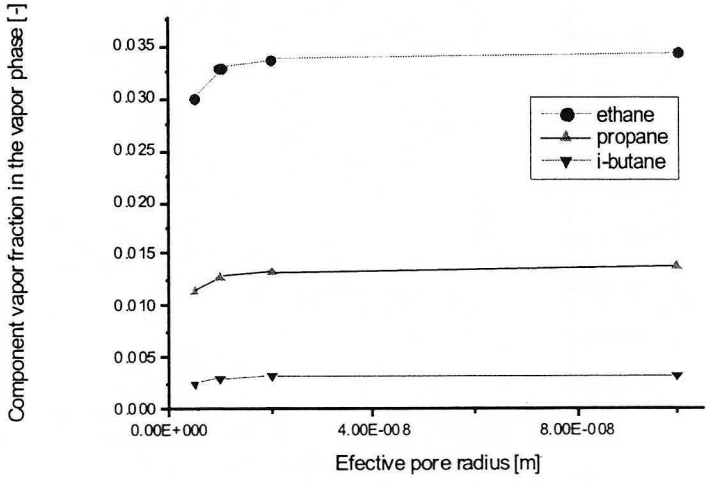

Fig. 18. Change of intermediated component fraction in the vapor phase as a function of pore radius for the mixture 2 (366.6 K, 210 bar — flat surface)

Rys. 18. Zmiana zawartości pośrednich składników roztworu w fazie parowej w funkcji promienia porowego dla roztworu 2 (366,6 K, 210 bar — dla fazy gazowej)

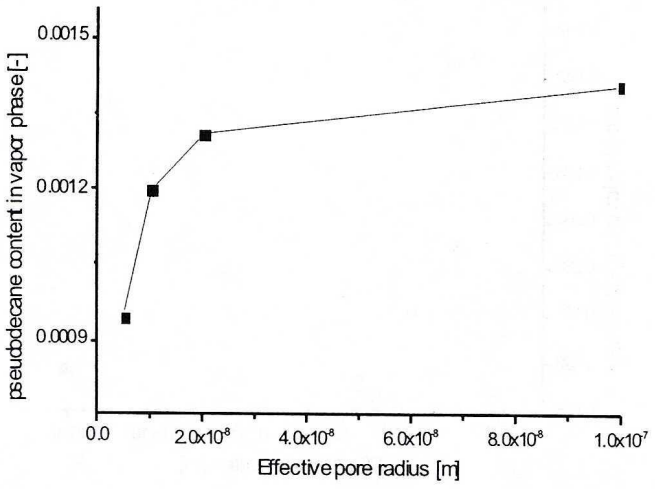

Fig. 19. Change of pseudo-decane fraction in the vapor phase as a function of pore radius for the mixture 2 (T = 366.6 K, 210 bar — flat surface)

Rys. 19. Zmiana zawartości frakcji pseudodekanu w fazie parowej w funkcji promienia porowego dla roztworu 2 (366,6 K, 210 bar — dla fazy gazowej)

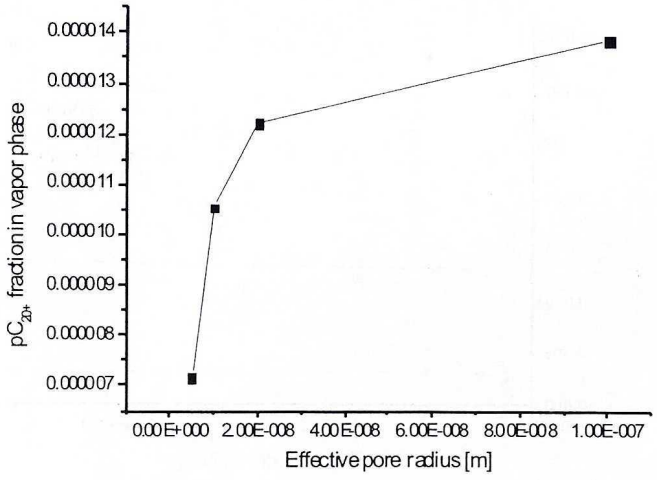

Fig. 20. Change of pC_{20+} fraction in the vapor phase as a function of pore radius for the mixture 2 (366.6 K, 210 bar — flat surface)

Rys. 20. Zmiana zawartości frakcji pC_{20+} w fazie parowej w funkcji promienia porowego dla roztworu 2 (366,6 K, 210 bar — dla fazy gazowej)

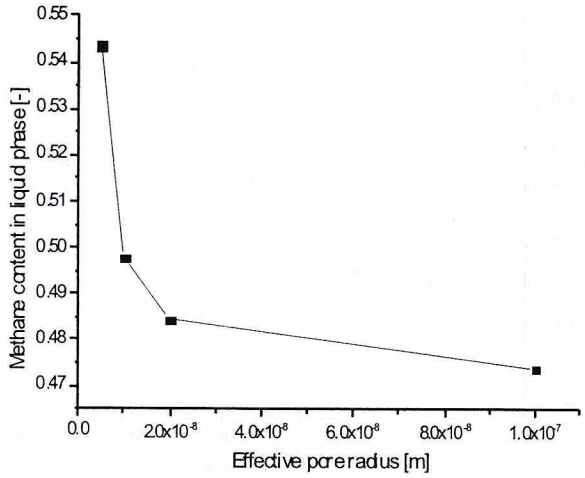

Fig. 21. Change of methane content in the liquid phase as a function of pore radius for the mixture 2 (366.6 K, 210 bar — flat surface)

Rys. 21. Zmiana zawartości metanu w fazie ciekłej w funkcji promienia porowego dla roztworu 2 (temperatura 366,6 K, ciśnienie 210 bar — dla powierzchni płaskiej)

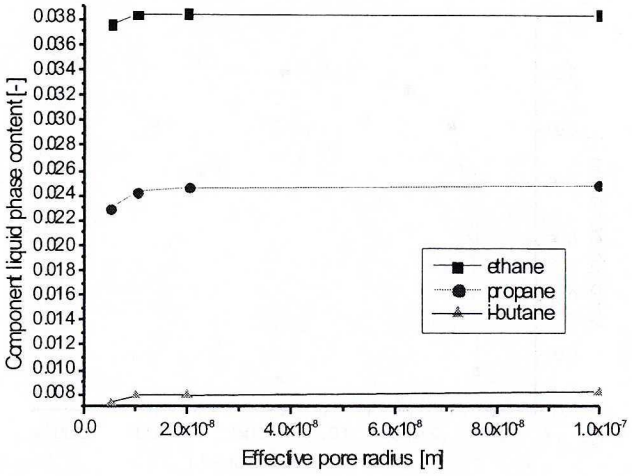

Fig. 22. Change of intermediate components content in the liquid phase as a function of pore radius for the mixture 2 (366.6 K, 210 bar — flat surface)

Rys. 22. Zmiana zawartości pośrednich składników roztworu w fazie ciekłej w funkcji promienia porowego dla roztworu 2 (temperatura 366,6 K, ciśnienie 210 bar — dla powierzchni płaskiej)

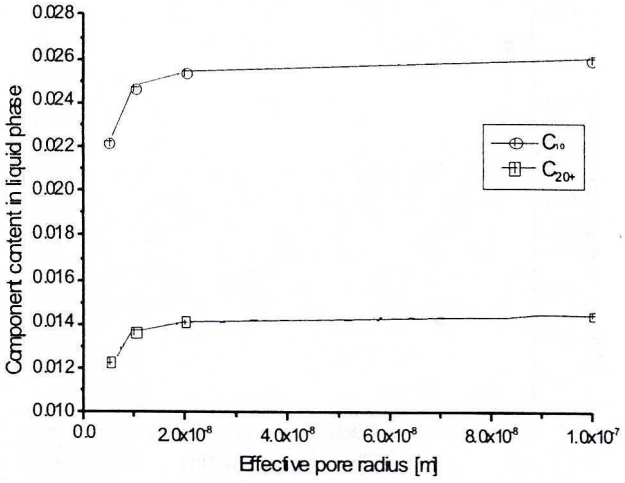

Fig. 23. Change of pC_{10} and pC_{20+}components content in the liquid phase as a function of pore radius for the mixture 2 (366.6 K, 210 bar — flat surface)

Rys. 23. Zmiana zawartości pseudoskładników pC_{10} i pC_{20+} w fazie ciekłej w funkcji promienia porowego dla roztworu 2 (temperatura 366,6 K, ciśnienie 210 bar — dla powierzchni płaskiej)

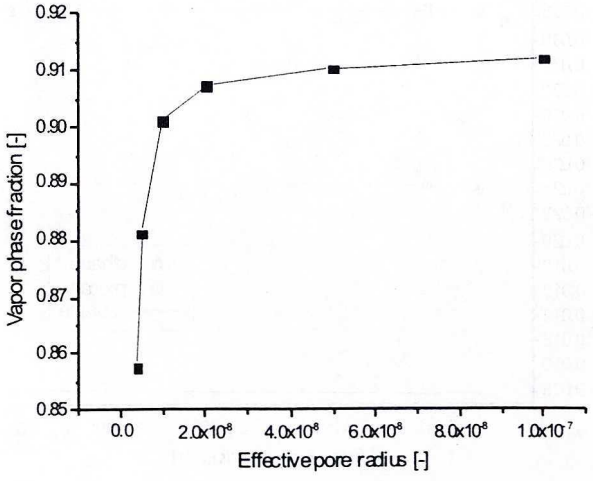

Fig. 24. Impact of pore radius on vapor phase fraction of mixture 3 at 200 bar (flat surface) and 402 K

Rys. 24. Wpływ promienia porowego na udział fazy gazowej roztworu nr 3 przy ciśnieniu 200 bar (płaska powierzchnia) i w temperaturze 402 K

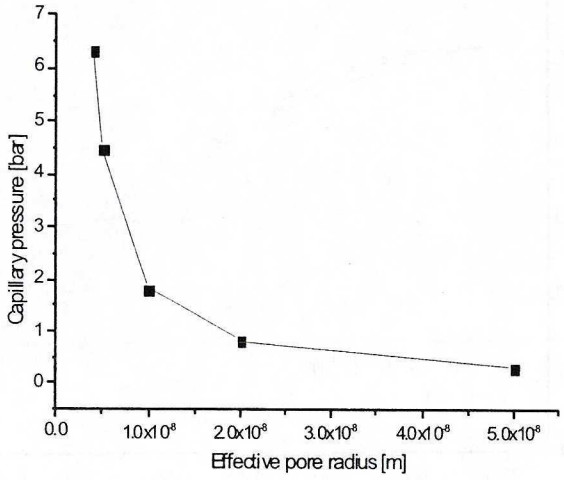

Fig. 25. Impact of pore radius on capillary pressure of mixture 3 at 200 bar and 402 K

Rys. 25. Wpływ promienia porowego na ciśnienie kapilarne roztworu nr 3przy ciśnieniu 200 bar (płaska powierzchnia) i w temperaturze 402 K

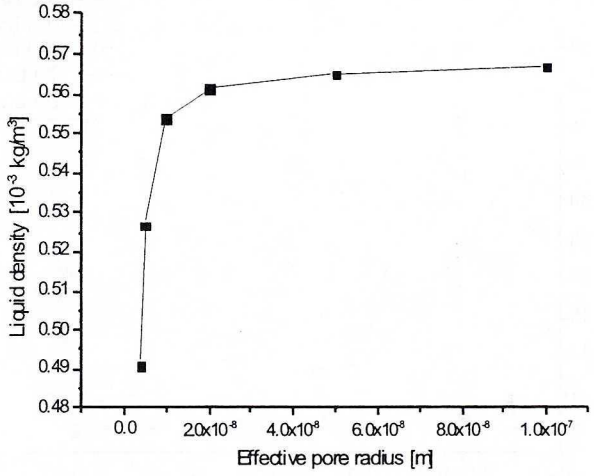

Fig. 26. Impact of pore radius on liquid density of mixture 3 at 200 bar and 402 K

Rys. 26. Wpływ promienia porowego na gęstość fazy ciekłej roztworu nr 3 przy ciśnieniu 200 bar (płaska powierzchnia) i w temperaturze 402 K

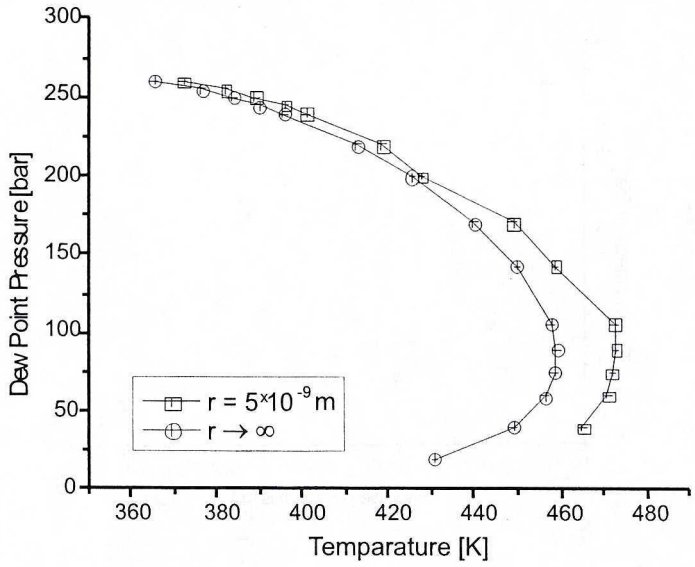

Fig. 27. Impact of pore radius of porous media on phase boundary movement (mixture 3) (T = 402 K)

Rys. 27. Wpływ promienia porowego na przesunięcie krzywej nasycenia (rosy) roztworu nr 3 (T = 402 K)

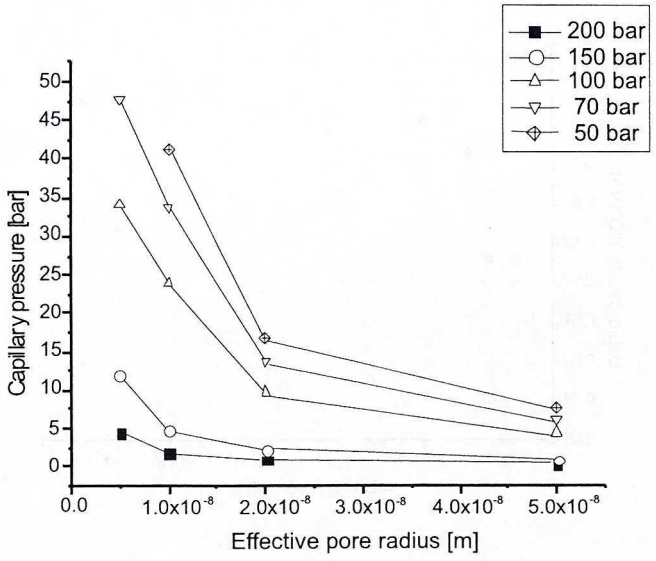

Fig. 28. Impact of pore radius and pressure of system (flat surface) capillary pressure near boundary (mixture 3) (T = 402 K)

Rys. 28. Wpływ promienia porowego i ciśnienia układu (dla powierzchni płaskiej) na ciśnienie kapilarne roztworu nr 3 (T = 402 K)

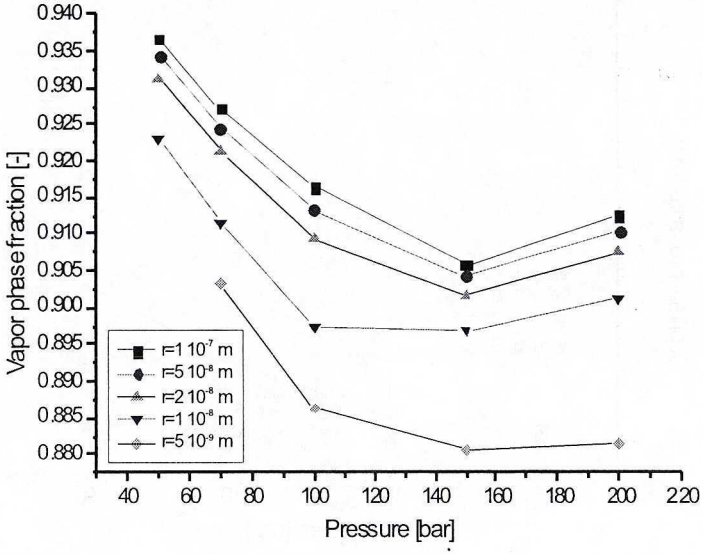

Fig. 29. Impact of pore radius and pressure of system (flat surface) on vapor phase fraction (mixture 3) (T = 402 K)

Rys. 29. Wpływ promienia porowego i ciśnienia układu (dla powierzchni płaskiej) na udział fazy gazowej dla roztworu nr 3 (T = 402 K)

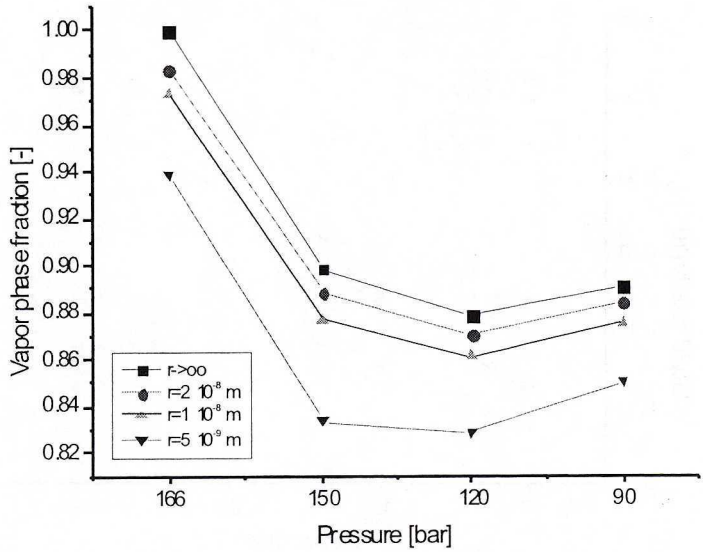

Fig. 30. Impact of pore radius and pressure of system (flat surface) on vapor phase fraction (mixture 1) (T = 473 K)

Rys. 30. Wpływ promienia porowego i ciśnienia układu (dla powierzchni płaskiej) na udział fazy gazowej roztworu nr 1 (T = 473 K)

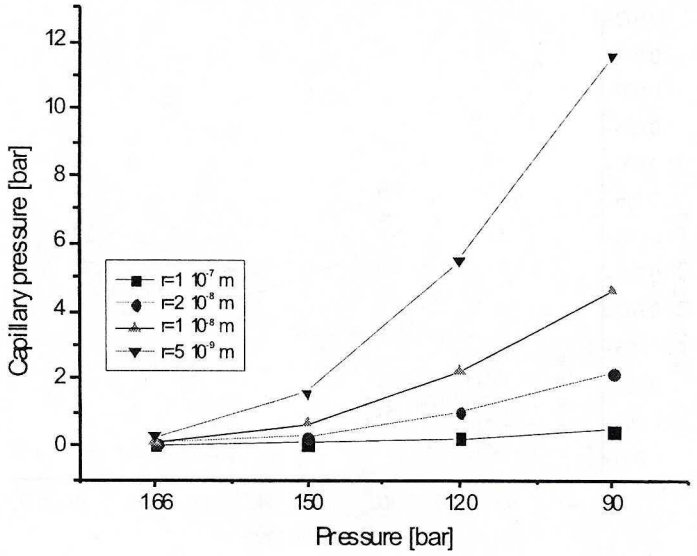

Fig. 31. Impact of pore radius and pressure of system (flat surface) on capillary pressure (mixture 2) (T = 366 K)

Rys. 31. Wpływ promienia porowego i ciśnienia układu (dla powierzchni płaskiej) na ciśnienie kapilarne roztworu nr 2 (T = 366 K)

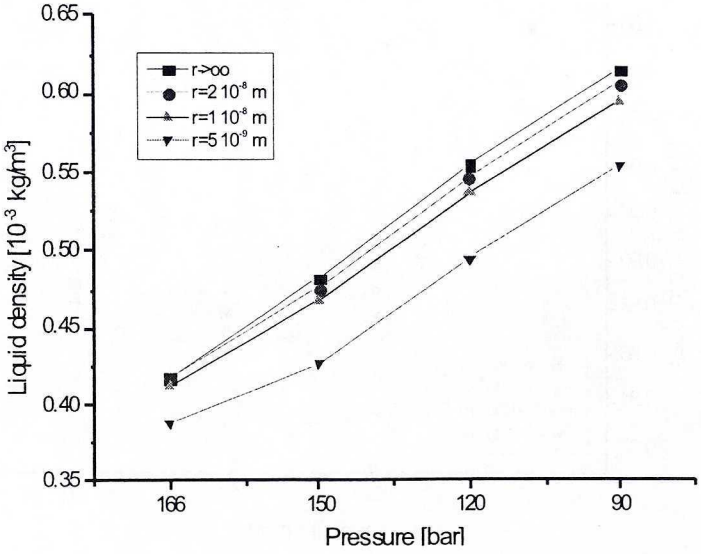

Fig. 32. Impact of pore radius and pressure of system (flat surface) on liquid density (mixture 2) (T = 366 K)

Rys. 32. Wpływ promienia porowego i ciśnienia układu (dla powierzchni płaskiej) na gęstość fazy ciekłej roztworu nr 2 (T = 366 K)

Fig. 26 shows the effect of pore radius on the vapour phase fraction of mixture 3 at 200 bar and 402 K and Fig. 27 the impact of pore radius on the capillary pressure in the same mixture. The influence of pore radius on the liquid density of mixture 3 at 200 bar and 402 K is presented in Fig. 28. Fig. 29 shows the impact of the pore radius of porous media on phase boundary movement (mixture 3), The influence it of pore radius on cricondenterm movement is evident. Fig. 30 shows the impact of the pore radius and pressure of the porous media system on the capillary pressure near the boundary of mixture 3. Vapour fraction changes in the presence of curvature of the porous media may be seen in Fig. 31. The impact of the pore radius and pressure of the porous media system (flat surface) on the vapour phase fraction (mixture 1) (T = 473 K) is depicted on Fig. 32.

Conclusions

The laboratory investigation cannot qualify and quantify predictions of VLE phenomena in tight sandstone cores. The dominant gravitational force mask the fully curved interfacial phenomena in the horizontal core experiments. The results obtained from previous Russian and Canadian works are not representative for typical natural--state porous media (Dannesh, Ping). The results of the laboratory work of Guo showed the great influence of reservoir the pore pressure, as opposed to dew pressure in the results of laboratory experiments. This may indicate that the equilibrium time needed to fulfil the thermodynamic requirement was too low during experiments.

The interfacial curvature phenomena have a negligible influence on PVT and VLE properties in high-permeability clean sandstones. In real reservoir conditions one may expect a curved surface to exist with an average hydraulic radius of the order of 1–5 μm (Lee 1989). It is equivalent to a local permeability of $0.1–0.2 \cdot 10^{-3}$ μm^2 (0.1–0.2 mD). For the mentioned hydraulic radius it is necessary to take the capillary effects into consideration when the VLE phase envelope is calculated.

The presented algorithm make possible to account capillary — adsorption effects during VLE computation of multicomponent mixture.

Advantages of the new algorithm: It is not necessary to compute saturation pressure (flat surface or curved surface) for Capillary Vapour Liquid Equilibria. No additional assumptions according to saturation pressure liquid composition need be made.

Diagrams 7–32 show two principal phenomena related to bulk dew and bubble--point curves. It is evident that movement of the cricondenbar outside the flat surface (bulk) phase boundary occurs. The movement may be significant — in the cited example the difference is 13K (Fig. 27). In the upper part of the curve below the critical point a diminished effect of curvature is observed. This is caused by lowering of surface tension (and capillary pressure) in the vicinity of the critical point. The opposite effect concerning the shape and position of the capillary condensation bubble curve is observed in Figs. 15–16. In the case of Hoffman et al. (1953) fluid (mixture 2) the lowering of pressure is about 23 bar, which is equivalent of 10% of the saturation pressure (in very tight rock — $r = 50$ nm). A similar effect of lowering of the

impact of the curvature may be observed on the right side of the critical point — see Fig. 27.

The importance of the curvature of porous media is evident at an average radius of 100 Angstrđms (see Figs. 7–16). The main factor governing the lowering of the influence of capillarity on the phase boundary is surface tension. The effect of curvature of porous media thus will be evident in the vicinity of the lower part of the dew and bubble curve. It seems evident that a stronger effect is observed in mixtures with a higher content of heavy fraction C_{10+} in the mixture.

The effect of capillary condensation makes the methane content increase (by up to 7%) — and sometimes ethane — in the vapour phase. There is a significant diminishing of the heavy component (i.e. C_{10}) which is selectively adsorbed and condensed on pore walls. A similar effect may take place for waxes and asphalt components in the mixture. The reduction of the decane fraction content is up to 13%. The composition of all other components is slightly lower in the vapour phase, but the difference is almost negligible.

A significant increase of methane content is observed in the liquid phase (i.e. from 47% up to 54%) and a very small or insignificant change of composition in ethane, propane, butane etc. in a high-pressure (210 bar) system. The relatively high impact of pore curvature is evident on pseudo-components pC_{10} and pC_{20+} (a decrease from 2.6% to 2.4% and from 1.4 to 1.2% — which is equivalent to 8 and 17%).

The observed change of liquid density is high. The reduction from 0.57 to 0.49 g/cm^3 is the result of changes of composition in the liquid phase and an increase of methane content (up to 14%).

The observed capillary effects may indirectly influence the reserves in tight rocks, part of the resources being permanently adsorbed in the pore structure, or desorbed at a very late stage of exploitation.

REFERENCES

Abual Al-Rub F.A., Datta R., 1998. Theoretical Study of Vapor Pressure of Pure Liquids in Porous Media. Fluid Phase Equilibria Vol. 147, p. 65–83.

Adamson A.W.,1990. Physical Chemistry of Surfaces. J. Wiley & Sons Inc.

Ahmed T., 1989. Phase Hydrocarbon Equilibria. Gulf Publishing Co., Tulsa.

Ahmed T., Cady, G., Story A., 1985. A Generalized Correlation for Characterizing the Hydrocarbon Heavy Fractions. Paper SPE 14266.

Amyx J.W., Bass D.M., Whiting R.L., 1960. Petroleum Reservoir Engineering Physical Properties. McCraw Hill Book.

Arbarbi S., Firoozabadi A., 1995. Near-critical Phase Behavior of Reservoir Fluids Using Equations of State. SPE Advanced Technology Series Vol. 3, No. 1, p. 139–145.

Behrens R., Sandler S., 1986. The Use of Semi-continuous Description to Model the C7+ Fraction in Equation of State Calculation. Paper SPE/DOE 14925.

Bertrand E., Bonn D., Broseta D., Meunier J., 1999. Wetting of Hydrocarbon Mixtures on Water Under Varying Pressure or Composition. Journal of Petroleum Science Vol. 24 (1999), p. 221–230.

Brusilovsky A.I., 1990. Mathematical Simulation of Phase Behavior of Natural Multicomponent System of High Pressure Using Equation of State. SPE 20180.

Causin E., Consoloni C., 1996. Evaluation of Heterogeneities & Composition Profiles of Hydrocarbon Mixtures in Reservoir: A New Analytical Approach. SPE 96824.

Creek J.L., Sakrader M.L., 1985. East Painter Reservoir: An Example at a Compositional Gradient from a Gravitational Field. SPE 14411.

Dąbrowski A., 2001. Adsorption — From Theory to Practice. Advances in Colloid and Interface Solids Vol. 93, p. 135–224.

Danesh A., Henderson G.D., Krinis D., Paden J.M., 1988. Experimental Investigation of Retrograde Condensation in Porous Media at Reservoir Conditions. SPE 18316.

Danesh A.S., Dandekar A.Y., Todal A.C., Sarkar R., 1991. A Modified Scaling Law and Parachor Method Approach for Improved Prediction of Interfacial Tension of Gas-Condensate System. SPE 2270.

Danesh A., Xu D.H., Todal A.C., 1990. An Evaluation of Cubic Equations of State for Phase Behavior Calculation Near Miscibility Conditions. SPE.

Defay R., Prigogine I., 1966. Surface Tension and Adsorption. Longmans, London.

Desbrandes R., Bassiouni Z., 1990. In Situ Wettability Determination in Gas Reservoirs. SPE 19058.

Dullien F.A.L., 1992, (ed). Porous Media. Fluid Transport and Pore Structure. 2nd Ed., Academic Press, Inc.

Economides M.J., Miller F.G., 1986. Geothermal Reservoir Evaluation Considering Fluid Adsorption and Composition. SPE Res. Eng., March 1986, p. 131–147.

Edmister W.C., 1961. Applied Hydrocarbon Thermodynamics. Gulf Publishing Company, vol. 1, Houston.

Edmister W.C., 1974. Applied Hydrocarbon Thermodynamics. Gulf Publishing Company, vol. 2, Houston.

Everett D.H., 1972. IUPAC manual of symbols and terminology for physicochemical quantities and units. App. II, Part I, Pure Appl. Chem. Vol. 21, p. 584–594.

Fanchi J., 1990. Calculation of Parachors for Compositional Simulation: An Updated. SPE Res. Eng., p. 433– 436, SPE 19453.

Firoozabadi A., 1988. Reservoir-Fluid Phase Behavior and Volumetric Prediction With Equation of State, J.P.T., April 1988, p. 397–406.

Firoozabodi A., Katz D.L., Soroosh H., Sajjadin A., 1988. Surface Tension of Reservoir Crude Oil/Gas Systems Recognizing the Asphalt in the Heavy Fractions. SPE.

Greenkorn R.A., 1983. Flow Phenomena in Porous Media. Dekker, New York.

Guo P., Sun L.T., Sun L., 1996. Studies of the Effect of Capillary Pressure on Condensate Oil & Gas Phase Behavior in Porous Media. [In:] Guo P., Sun L., Li S., 1996, SPE 35644.

Guo T.M., 1983. Vapor — Liquid Equilibrium & Rectification of Multicomponent, Being, Chem. Industry Publishing. [In:] Guo P., Sun L., Li S., 1996, SPE 35644.

He G.S., Reservoir Physics, Petroleum Industry Publishing House, 1994. [In:] Guo P., Sun L., Li S., 1996, SPE 35644.

He G.S., Sun Le, Huang Y. et al., 1992. A Modified Cubic Equation of State and the Application to the Phase Equilibrium Calculations of the Gas Condensate Fields. SPE 22418.

He J.C., Li S.L. et al., Studies of Read Dew Point in Gas Condensate, Natural Gas Industry, 1995. [In:] Guo P., Sun L., Li S., 1996, SPE 35644.

Hocier L.,. Whitson C.H, 2000. Compositional Grading — Theory and Practice. SPE 63085.

Hoffman A.E., Crump J.S., Hocott C.R., 1953. Equilibrium Constants for Gas-Condensate System. Pet. Trans. AIME Vo. 198, p. 1.

Holt T., Linderberg E., Ratkje S.K., 1983. The Effect of Gravity and Temperature Gradients on Methane Distribution in Oil Reservoirs. SPE 11761.

Huang W.W., 1985. Some Experience with a Critical Reservoir Fluid. SPE 14415.

Hubert M.K., 1956. Darcy's Law and the Field Equations of State of Underground Fluids. Trans. AIME Vol. 198.

Huntington R.L., 1950. Natural Gas and Natural Gasoline. McGraw Hill Book Co.

Jhaveri B.S., Youngren G.K., 1988. Three Parameter Modification of the Peng Robinson Equation of State to Improve Volumetric Predictions. SPE Res. Eng., (Aug. 1988), p. 33.

Jun W.Y., Huang Y.Z., 1988. The Influence of Porous Media on Gas Liquid Phase Transition Process, Petroleum Exploration & Exploitation, 1988. [In:] Guo P., Sun L., Li S., 1996, SPE 35644.

Katz D.L., Firoozabadi A., 1978. Predicting Phase Behavior of Condensate/Crude Oil Systems Using Methane Interaction Coefficients. J.P.T. Vol. 20, p. 1649–1655.

Kingston P.E., Niko H., 1975. Development Planning of the Brent Field. 1975.

Kordas A.K., Magoulas S., Stamataki D. Tassios, 1995. Methane-hydrocarbon interaction parameters correlations for the Peng-Robinson and the t-mPR equation of state. Fluid Phase Equilibria Vol. 112, p. 33–44.

Lee S.T.,1989. Capillary — Gravity Equilibria for Hydrocarbon Fluids in Porous Media. SPE 19650.
Leverett M.C., 1941. Capillary Behavior in Porous Solids. Trans. AIME Vol. 142, p. 152–169.
Li D., 1994. Curvature Effect on the Phase Rule Fluid Phase Equilibrium. [In:] Guo P., Sun L., Li S., 1996, SPE 35644.
Martin J.J., 1979. Cubic equation of state-which? Ind. Eng. Chem. Fundam. Vol. 18, p. 81–97.
McCain W., 1990. The Properties of Petroleum Fluids. Tulsa.
Michelsen M.L, 1982a. The Isothermal Flash Problem I. Stability analysis. Fluid Phase Equilibria Vol. 8, p. 1–19.
Michelsen M.L, 1982b. The Isothermal Flash Problem I. Phase Split Calculation. Fluid Phase Equilibria Vol. 8, p. 21–40.
Michelsen M.L, 1985. Saturation Point Calculations. Fluid Phase Equilibria Vol. 23, p. 181–192.
Michelsen M.L., 1984. Calculation of Critical Points and Phase Boundaries in the Critical Region. Fluid Phase Equilibria Vol. 16 (1984), p. 57–76.
Montel F., Gouel P.L., 1985. Prediction of Compositional Grading in a Reservoir Fluid Column. SPE 14410.
Nagy S., 1992a. The Influence of Hydrocarbon Condensation on Natural Gas Throttling Temperature. Archiwum Termodynamiki Vol. 12, No. 1–4, p. 101–116.
Nagy S., 1992b. Isenthalpic Throttling Effect in Multiphase and Multicomponent Systems. Archiwum Termodynamiki Vol. 12, No. 1–4, p. 116–128.
Nagy S., 1996. The Modeling of the Composition Changes in the Gas-condensate System. Archives of Mining Sciences Vol. 41, Iss.3, p. 275–290 (in Polish).
Neveux A.R., Sakthikumar S., Noiray J.M., 1988. Delineation and Evaluation of North Sea Reservoir Containing Near — Critical Fluids. SPERE.
Oxford C.W., Huntington R.L., 1953. Vaporization of Hydrocarbons from an Unconsolidated Sand. Trans. AIME (1953) Vol. 198, p. 318–322.
Patel N.C., Teja A.S., 1982. A new cubic equation of state for fluids and fluids mixtures. Chem. Eng. Sci. Vol. 37, p. 463–473.
Pedersen K., Thomassen P., Fredenslund A., 1982. Phase Equilibria and Separation Processes. Report SEP 8207, Hojskole.
Pedersen K.S., Thomassen P.T., Fredenslund A., 1989a. On the Danger of Tuning Equation of State Parameters. SPE 14487.
Pedersen K.S., Thomassen P., Fredenslund A., 1996. Adjustment of C7+ Molecular Weights in the Characterization of Petroleum Mixtures Containing Heavy Hydrocarbons. Instituttet for Kemiteknit (papier SPE nr 16036).
Pedersen K.S., Fredenslund Aa., Thomassen P., 1989b. Properties of Oils and Natural Gases. Gulf Publishing Co., Houston, Tx.
Peneloux A., Rauzy E., Freeze R., 1982. A Consistent Correction for Redlich-Kwong-Soave Volumes. Fluid Phase Equilibria Vol. 8, p. 7–23.
Peng D.Y., Robinson D.B., 1976. A New Two Constant Equation of State. Ind. Eng. Chem. Fundam. Vol. 15, p. 59.
Ping Suo, Sundiongton, Li Shilan, Sun Lei, 1996. A Theoretical Study of the Effect of Porous Media on the Dew Point Pressure of a Gas Condensate. SPE 35644.
Razi M.R., Daubert T.E., 1980. Prediction of the Composition of Petroleum Fractions. Ind. Eng. Chem. Processs Des. Dev Vol. 19, p. 289.
Reid R.C., Modell M., 1974. Thermodynamics & Applications. Ch. 11, Prentice Hall.
Reid R.C., Prausnitz J.M., Polling B.E., 1987. The Properties of Gases and Liquids. McGraw Hill, New York.
Riemans W.R., Schulte A.M., de Jong L.N.J., 1988. Birba Field PVT Variations Along the Hydrocarbon Column and Confirmatory Field Tests. J.P.T., p. 83–88.
Sadyk K., Zade E.S., 1968. A Study of the Process at Equilibrium Rate Attainment During Condensate System. Neft i Gaz.
Sadyk K., Zade E.S., 1963. Determination of the Beginning of Condensation in the Presence of Porous Media. Neft i Gaz.
Saedi A., Handy L.L., 1985. Flow and Phase Behavior of Gas Condensate and Volatile Oil in Porous Media. SPE 4891.
Sarkar R., Dandesh A.S., Todd A.L., 1991. Phase Behavior Modeling of Gascondensate Fluids Using an Equation of State. SPE 22714.

Sassen R., 1988. Recent Hydrocarbon Alteration Sulfate Reduction and Formation of Elemental Sulfur and Metal Sulfide in Salt Dome Cap Rock, Chemical Geology.

Satik C., Horne R.N., Yortsos Y.C., 1995. A Study of Adsorption of Gases in Tight Reservoir Rocks. SPE 30732.

Shang S., Horne R.N., Ramey H., 1995. Water Vapor Adsorption on geothermal Reservoir Rocks. Geothermics Vol. 24, No. 4, pp. 523–540.

Shapiro A.A., Stanby E.H., 1996. Effect of Capillary Forces & Adsorption on Reserves Distributions. SPE 36922.

Siemek J., Dawidowicz, S. Nagy S., Rybicki C., 1987. Thermodynamic Problems of Hydrocarbon Reservoir Exploitation. Materiały XII Zjazdu Termodynamików, Częstochowa-Kozubnik, p. 581(In Polish).

Siemek J., Nagy S., 2001. The Early Time Condensation In The Near Well Zone During Non-Stationary and Non-Isothermal Flow of Gas Condensate System. Archives of Mining Vol. 20, Iss. 3.

Sigmund P.M., Dranchuk P.M., Morrow N.R., Purvis R.A., 1973. Retrograde Condensation in Porous Media. SPEJ.

Sim W.J., Daubert T.E., 1980. Prediction of Vapor-Liquid Equilibria of undefined Mixtures. Ind. Eng. Chem. Process Des. Dev. Vol. 19, 1090, p. 386–393.

Smith L.R., Yarborough L., 1968. Equilibrium Revaporization of Retrograde Condensate by Dry Gas Injection. SPEJ (March 1968), p. 87–94.

Soave G., 1972. Equilibrium Constants from a Modified Redlich-Kwong Equation of State. Chem. Eng. Sci. Vol. 27, p. 1197.

Soereide I., Whitson C.H., 1990. Discussion of a Systematic and Consistent Approach to Determine Binary Interaction Coefficients for the Peng-Robinson Equation of State. SPE Reservoir Engineering, May 1990, p. 260–261.

Stamataki S.K., Magoulas K.G., 2001. Characterization of Heavy Undefined Fraction. SPE 64996.

Stryjek R., Vera J.H.,1986. PRSV: an Improved Peng-Robinson Equation of State for Pure Compounds and Mixtures. Can. J. Chem. Eng. Vol. 64, p. 323–333.

Suo P., Sun L.T., Sun L., Studies of the Effect of Capillary Pressure on Condensate Oil & Gas Phase Behavior in Porous Media. Petroleum Exploration & Exploitation, 1994. [In:] Guo P., Sun L., Li S., 1996, SPE 35644.

Tindy R., Raynal M., 1966. Are Test Cell Saturation Pressures Accurate Enough? Oil and Gas Journal.

Tissot B.P., Welte D.M., 1978. Petroleum Formation & Occurrence Springer Verlag.

Trebin R.A., Zadora G.I., 1968. Experimental Study of the Effect of Porous Media on Phase Changes in Gas Condensate Systems. Neft i Gaz.

Tsai J.-Ch., Chen Y.-P., 1998. Application of a volume-translated Peng-Robinson equation of state on vapor-liquid equilibrium calculations. Fluid Phase Equilibria Vol. 145, p. 193–215.

Voros N., Stamataki S., Tassios D.T., 1994. Effect of Translation on the Prediction of Saturated Densities of Binary Mixtures with a Peng-Robinson equation of state. Fluid Phase Equilibria Vol. 96, p. 51–63.

Weinang C.F., Cordell J.C., 1949. Revaporization of Butane and Pentane from Sand. Trans. AIME (1949) Vol. 179, p. 303–312.

Weinaug C.F., Katz D.L., 1943. Surface Tension of Methane-Propane Mixtures. I&EC, p. 239–246.

Wheaton R.J., 1988.Treatment of Variations of Composition with Depth in Gas Condensate Reservoir. SPE 18267.

Whitson C.H., 1985. Critical properties estimation from an Equation of State. SPE 12634.

Whitson C.H., 1983. Characterizing Hydrocarbon Plus Fractions. SPEJ (Aug. 1983), p. 683.

Whitson C.H., 1985. Properties on Equation of State Predictions. SPEJ (Dec. 1984), p. 685.

Wiliams J. K., Dawe R.A., 1989. Near-Critical Condensate Fluid Behavior in Porous Media — A Modified Approach. SPE Res. Eng., May 1989, p. 221–227.

Win F.W., 1957. Physical Properties by Nomogram Pet. Refiner Vol. 36, p. 157.

Yan Q.L., He Q.X., 1988. Phase Change Characterization of Condensate Oil and Gas in Porous Media. [In:] Guo P., Sun L., Li S., 1996, SPE 35644.

Yortsos Y.C., A.K. Stubos, 2001. Current Opinion in Colloid & Interface Science Vol. 6, p. 208–216.

Yu J.-M., Lu B.C.-Y., 1987. A three-parameter cubic equation of state for asymmetric mixture density calculations. Fluid Phase Equilibria Vol. 34, p. 1–19.

Zhu W.Y., Huang Y.Z., 1988. The Influence of porous media on gas-liquid phase transition process. [In:] Guo P., Sun L., Li S., 1996, SPE 35644.

REVIEW BY: PROF. DR HAB. INŻ. JAKUB SIEMEK, KRAKÓW

Received: 26 March 2002